



PROJECT FINAL REPORT

Grant Agreement number: **611019**

Project acronym: **PiezoMAT**

Project title: **High-resolution fingerprint sensing with vertical piezoelectric nanowire matrices**

Funding Scheme: **FP7 [ICT-2013.3.3]**

Period covered: from **November 1st 2013** to **June 30th 2017**

Name of the scientific representative of the project's co-ordinator¹, Title and Organisation:

Dr Antoine Viana, Commissariat à l'Energie Atomique et aux Energies Alternatives

Tel: **+33 (0)4 38 78 99 86**

Fax:

E-mail: **antoine.viana@cea.fr**

Project website : **<http://www.piezomat.eu>**

¹ Usually the contact person of the coordinator as specified in Art. 8.1. of the Grant Agreement.

1. Executive summary	3
2. Summary description of the project context and the main objectives	4
The PiezoMAT sensor concept	4
Scientific and Technical objectives of the PiezoMAT project	5
3. Main Scientific & Technical results/foregrounds	6
3.1 Introduction	6
3.2 Architecture I: nano-deposited electrodes	7
Architecture-I devices: technical challenges and solutions	8
Nano deposition of the electrodes	9
Structural and electrical properties of contacted ZnO NW devices.	9
Positioning Architecture 1 within PiezoMAT	11
3.3 Architecture II: bottom-bottom contacted nanowires	11
Seed layer deposition using PLD	12
Chip processing and NW growth	13
Encapsulation of A-II chips	13
Electromechanical and structural characterization of the A-II chips	14
Multiphysics FEM modelling of the bottom-bottom contacted ZnO NWs for bending force sensing	16
3.4 Architecture III: top-bottom contacted nanowires	19
Si carrier-chip fabrication	19
Nanowires growth on architecture III chips	21
Specific polymer matrix	22
Fabrication of the top electrodes for A-III chips	23
A-III-R3 sensor (alternative version): fabrication and tests	24
A-III-R1, R2 & R3 sensors: functionality demonstration	28
FEM modelling of A-III type ZnO NWs for compression force sensing (A-III)	29
3.5 Conclusion	33
4. Potential impact, main dissemination activities, exploitation of results	35
Scientific and technical impact to the research market	35
Socio-economic impact and the wider societal implications of the project	37
5. Use and dissemination of foreground	40
6. Report on societal implications	48

1. Executive summary

The PiezoMAT Project was a 44 months EU FP7 project running from 2013 to 2017. It brought together 8 partners from research and development centres and small and medium enterprises from across the EU. The aim of the PiezoMAT project is to make the proof of concept of a new technology for developing a high-resolution fingerprint sensor, based on a matrix of interconnected piezoelectric nanowires (NWs). PiezoMAT proceeds by local deformation of an array of individually contacted piezoelectric NWs (*pixels*), grown on patterned silicon wafers, and encapsulated into a polymer matrix. The characteristic size of a nanowire allows resolution of >1000 dpi. Hence, the long term objective of PiezoMAT is to offer high performance fingerprint sensors with a minimal volume occupation for integration into built-in systems. Such systems should compete on the market with the best existing products. Since charge collection efficiency is very dependent on the electrode configuration on each nanowire, PiezoMAT explored 3 possible configurations associated with levels of technological challenges and risks.

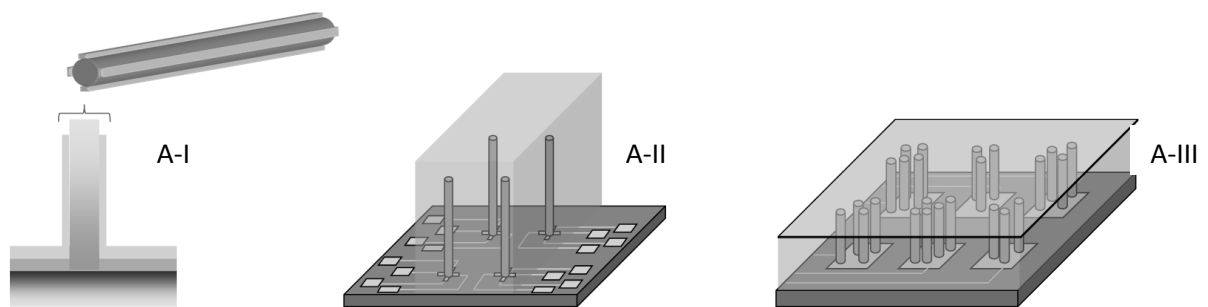


Figure 1: Electrode on NW configurations foreseen within PiezoMAT. (Architecture 1, A-I) Single NW contacting by direct localised metal deposition; (Architecture 2, A-II) Contacted NWs on chip with a 4-bottom contact configuration and an encapsulating polymer; (Architecture 3 A-III) Contacted NWs on chip with a top-bottom contact configuration and an encapsulating polymer in the inter-electrode spacing.

The outcome of the project is the fabrication of a demonstrator embedding a silicon chip with 250 pixels, and associated electronics for signal collection and treatment. This configuration does not allow a maximum nanowires integration density but was designed to yield sufficient resolution (≥ 1000 dpi) to demonstrate the concept and major technological achievements. Long term developments will pursue full electronics integration for an optimal sensor resolution.

Valuable experience was gained in several scientific and technological areas, such as seed layers optimization, ZnO NW growth on patterned ZnO/Si substrates, mathematical modelling of piezoelectric mechanisms along with polymer technology and characterization method development. The research and deliverables from the PiezoMAT project have been disseminated via publications in scientific journals, conference papers, and PiezoMAT-Workshop event within Eurosensors2016 Conference in Budapest.

2. Summary description of the project context and the main objectives

Biometrics is part of our everyday lives and is bound to become increasingly wide-spread in our society, inherently of novel intensive smart-device-connected behaviours and networking activities which require enhanced security measures for identification (ID) protection. Forensic and civil identification as well as rigorous access control remain large segments of the biometrics market, whereas consumer identification applications, notably in terms of access to banking and health care, are emerging. Given the zero fault tolerance for these applications, manufacturers turn towards innovative solutions for fingerprint sensors which enable large area scanning on small volume terminals, with very high spatial resolution, using scalable and portable technologies and complying with governmental requirements.

The PiezoMAT sensor concept

The PiezoMAT concept is to design a new technology of fingerprint sensor based on a matrix of inter-connected piezoelectric nanowires. The direct consequence of integrating nano-objects rather than conventional microsystems is to diminish the size of individual pixels enabling larger integration densities, and thus, higher spatial resolutions.

Currently available products exploit mainly capacitive and optical technologies. Achievable resolutions using these technologies are of the order of 500 dpi, which corresponds to $50 \times 50 \mu\text{m}^2$ individual pixel size. Such resolutions enable **level 1** and **level 2** fingerprint feature detection, respectively *singular points* and *minutiae points* (*ridge ending* and *bifurcations*). Performance and security increase can be expected from **level 3** feature detection (*ridge shapes and pores*). However, current fingerprint technologies are not dimensioned to detect such features, which require essentially a higher number of pixels per image. Developments related to the decrease of pixel size through the miniaturisation of sensing elements are slow and costly. Moreover, they exploit mostly top-down approaches (i.e. reducing the minimum feature size for an existing technology). New developments such as Thin-Film Transistor (TFT) and flexible (Flex) technologies open up the way towards compact and low cost devices, but should be fitted to the fingerprint applications. As a result, nowadays, there is an explicit need among manufacturers to go beyond the state-of-the-art of fingerprint sensors, possibly through highly innovative routes, in order to reach higher spatial resolution of images.

The PiezoMAT concept highlights a completely new *bottom-up approach* for increasing pixel integration density on a chip, thus solving the abovementioned resolution limitation. Ultimately, individual pixels of the PiezoMAT matrix will be fabricated from nano-objects. This approach reduces the pixel size drastically, well below $50 \times 50 \mu\text{m}^2$. In the case of the identified fingerprint sensor application, nano-objects are vertically grown ZnO NWs, which act as micro-(nano)-scale force sensors being equidistantly distributed on the sensor surface. Indeed, the mechanical deformation applied to each NW generates a change in electrical potential within the NW. Collecting the charges induced by strain in each NW of a 2D matrix enables to reconstruct a 3D deformation field corresponding to the fingerprint (the third dimension is given by the incremental potential value as a function of the deformation rate). The project focuses on the charge collection phase, which is the heart of the PiezoMAT concept.

From a technological point of view, the PiezoMAT concept addresses some fundamental technical issues related to the fabrication and interconnection of individual nano-pixels. Here, nanotechnology meets serious limitations, especially, when it comes to the high grade of system integration. Positioning, contacting, encapsulating and packaging nano-pixels and communicating with them in a controlled and reproducible manner remain a challenge. Technological breakthroughs resulting from collective effects of large ensembles

of NWs (or nanoparticles) have got some success on the market in the past few years. These are the third generation solar cells, high-developed-surface chemical sensors and energy conversion devices as well as carbon nanotubes for material reinforcement and water filtration membranes, etc. In the most cases, nano-objects are part of a larger system and sometimes play a completely passive role, for which no individual addressing is required. Introducing functionality (i.e. sensing) implies to integrate well-suited electronics and packaging solutions, which are the main drawbacks for the nanotechnologies. For all these reasons and due to some past reticence to introduce nanomaterials within usual industrial channels, individual nanoparticle functionalities remain under-exploited. Therefore, PiezoMAT consortium intends to demonstrate a compatibility of developed nanotechnologies with industrial applications targeted for large-volume consumer markets.

Scientific and Technical objectives of the PiezoMAT project

The overall technical objective of PiezoMAT is a development of effective technological solution in order to increase 3D resolution of fingerprint sensor. This has been realized via a drastic pixel size decrease provided by the nano-technology. In particular, a *bottom-up* fabrication approach was developed and applied to fabricate addressable, ordered arrays of vertically aligned NWs where an analogue signals were extracted from each NW individually. Success is to be evaluated on a reduced-size, packaged system of sensors, based on the demonstration of a significant performance increase in terms of resolution as compared to current market specifications.

It is to be noted that the demonstrator device developed within the present project, and in particular the packaging and interfacing solutions (without fully-integrated electronics), are an intermediary step towards the market product. As such, in addition to expected resolution-wise performances, they must also provide sufficient sensitivity to validate fingerprint reconstruction in the final phase of the project. Nevertheless, sensitivity is another sensor parameter, whose optimisation is not foreseen in the course of the present project. Similarly, full 3D integration of associated electronics is a further stage of the system development and is also out of the scope of the present project.

The aims of the PiezoMAT project can be summarised as follows:

- PiezoMAT proposes a new, scalable technology for fingerprint sensors, ensuring sufficient resolution to detect level 3 minutiae such as pores and ridge edges. Such a level of resolution considerably strengthens the reliability of fingerprint reading and enables security reinforcement regarding biometric identification, which is being more and more broadly used for everyday life purposes in our societies.
- PiezoMAT exploits multidisciplinary competences in nanoscale fabrication, characterisation and integration in a constructive and efficient manner.
- PiezoMAT **provides** – in addition to a fingerprint sensor demonstrator – exploitable data at several stages of its development. Technological processes (multiple contacting of NWs, localised growth, packaging solutions), characterisations (multi-scale electro-mechanical measurements) and associated analyses (multi-physics modelling, find a particular resonance in other ICT domains, for example in the broadly investigated field of nanoscale energy harvesting using piezoelectric NWs)
- PiezoMAT **explores** an innovative bottom-up integration approach which is not limited either to piezoelectric NWs or to fingerprint sensors. Through successive technological developments, PiezoMAT addresses broader stakes in nanotechnology integration and aims to validate methodologies, which **open up** immediate and longer term innovation routes in ICT, through additional performance increase (e.g. sensitivity) or functionality diversity (e.g. actuation).

3. Main Scientific & Technical results/foregrounds

3.1 Introduction

To address the rapidly growing need for rapid, reliable, and full proof personal identification, authentication systems will necessarily require a *biometric* component. *Enrolment* and *identification* are the two primary processes involved in a biometric security system. During enrolment, biometric data are captured from a subject using a *physical sensor*, and related raw information is digitized and stored in the database. During identification, biometric information is detected by the sensor and compared *in situ* against the database through pattern recognition techniques.

Biometric systems use persons' unique and time-invariant physical characteristics to determine the identity, e.g. fingerprints, face, iris, etc. Fingerprints have the distinctive advantages when compared with other modalities: well-developed and highly reliable identification algorithms along with small dimensions of the sensor which can be implemented into pocket-sized terminals. Fingerprints are made of a unique series of ridges and valleys (minutiae) on the finger surface. Fingerprint friction ridge details are generally described in a hierarchical order at three levels, namely: Level 1 (pattern: arches, loops and whorls), Level 2 (minutiae points) and Level 3 (pores and ridge shape). Minutiae and patterns are the distinctive 3D features with characteristic dimensions ranging from mm to several μm scales. Therefore, in fingerprint identification system, overall performance is primarily determined by two factors: the physical characteristics of the sensor, i.e. spatial resolution, sensitivity, signal/noise ratio, along with accuracy of pattern recognition algorithms. Main-stream fingerprint sensor technologies allow high-quality recognition of minutiae-related data with a 2D resolution of ~ 500 dpi covering the fingerprint between 15 to 25 mm^2 . The typical examples are optical imaging and solid-state capacitive sensors based on silicon CMOS chips. Their distinctive futures, however, are a limited lateral resolution and a lack of 3D data. Emerging fingerprint technologies, such as ultrasound image detection and direct-touch sensing based on in-finger light dispersion, can either recognize 3D pattern or reach lateral resolution over 1000 dpi, respectively, but not simultaneously.

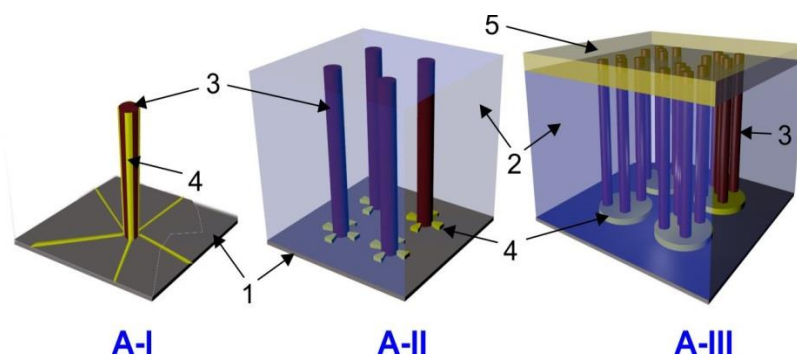


Figure 2: Schematic representation of three different sensing architectures (A-I, A-II & A-III) realized in the PiezoMAT project. Here, 1 is a patterned silicon chip (carrier), 2 is an insulating polymer matrix, 3 is the ZnO NW, 4 are the charge collecting electrodes, and 5 is a top contact for the A-III chip.

A newly developed PiezoMAT sensor allows combining these two distinctive features in one highly integrated device. PiezoMAT sensor is based on direct-touch sensing principle and based on a large number of identical micro-detectors combined into an addressable 2D matrix. Its lateral (2D) resolution is determined merely by the density of array elements (the pixels) micro-fabricated on the patterned CMOS chip (the carrier). The distinctive feature of the PiezoMAT sensor is related to the unique construction of the constituent pixels. Each of them consists of a bunch of ZnO nanowires (NWs) - piezo-semiconductor nano-devices capable to change electrical characteristics depending on their internal strain, e.g. upon applying mechanical load to the pixel. Therefore, each pixel acts as a “displacement” sensor delivering the electrical signal proportional to the

locally applied force. If the finger is in a direct-touch with the sensor array, the changes in the electrical signal collected from the pixels corresponds directly to the depth profile of the finger surface, e.g. ridges and valleys causing higher and lower strain in the NWs, respectively, allowing reconstructing the 3D profile of fingerprint in the real-time.

For the piezo-semiconducting sensors, charge collection efficiency is very dependent on the electrode configuration on each NW. PiezoMAT explores several possible configurations associated with a gradually increasing level of technological challenges and risks, with a strong focus on developing reliable device design tools for present and future application-related adaptability. For this purpose, three different architectures of the sensor have been designed, fabricated and tested (see Fig. 1). Architecture I (A-I, research grade, TRL3) is described in Section 3.2. A-I comprises stand-alone ZnO NWs equipped with nano-electrodes fabricated by an electron-beam induced deposition. Architecture II (A-II, proof-of-concept grade, TRL4) is considered in Section 3.3. A-II represented by an addressable matrix of bottom-bottom contacted ZnO NWs allowing to demonstrate an ultra-high sensing resolution (>5000 dpi). Architecture III (A-III, prototype grade) is discussed in Section 3.3. A-III chips are equipped with an addressable matrix of top-bottom contacted ZnO NWs with a resolution of 1000 dpi and fabricated for the system prototype tests in an operational environment.

Targeted for the demonstration, A-III configuration does not allow for a maximum NW integration density as compared to A-II (5000 dpi). However, A-III is more feasible for fabrication, and is designed to yield sufficient resolution to demonstrate the concept, major technological achievements and actual performance enhancement as compared to the state-of-the-art fingerprint detectors.

3.2 Architecture I: nano-deposited electrodes

Initial numerical modelling of pure piezoelectric NWs performed by KTU showed that 2D bending of the ZnO NW induces opposite sign charges on diametrically opposite facets of a NW: a potential difference is measured between opposite facets in both directions of the plane via 6 diametrically opposite electrodes distributed along the perimeter of the NW. Hence, in an ideal electrode configuration (A-I, see Fig. 2), electrically insulated contacts should be developed along the full length (few micrometers) of the NW facets, hence achieving maximum charge collection. In comparison, A-II configuration allow collection of charges only at the bottom of the NW facets, limited by the height (few hundreds of nm) of the deposited contact metal.

Devices using arrays of vertical structures such as NWs and pillars have already been demonstrated and applied as vertically integrated field effect transistors, photovoltaic components, nano-generators and bio-chemical and mechanical sensors. In such devices contacts are normally developed at the tip and at the base of the vertical structures. The sidewall facets are typically tailored to achieve desired application e.g. gate layers for gate-all-around NW transistors, radial heterojunctions for NW photovoltaics or specific surface functionalities for bio-chemical sensing. In such devices, the sidewall facets of an assembly of vertical structures are modified around the whole perimeter. Addressing the need to contact individual facets of crystals, nano-manipulator driven electrical probes within an electron microscope have been used. Although extremely flexible, such approach is limited to the probe curvature and in the inability to predict the nature of the tip/facet interactions, which might have deterministic effect onto the performance of the devices. Until now no lithography-based approach for contacting individual sidewall facets of vertical structures has been demonstrated. When it is achieved, functional, high efficiency, vertical NW devices can be obtained.

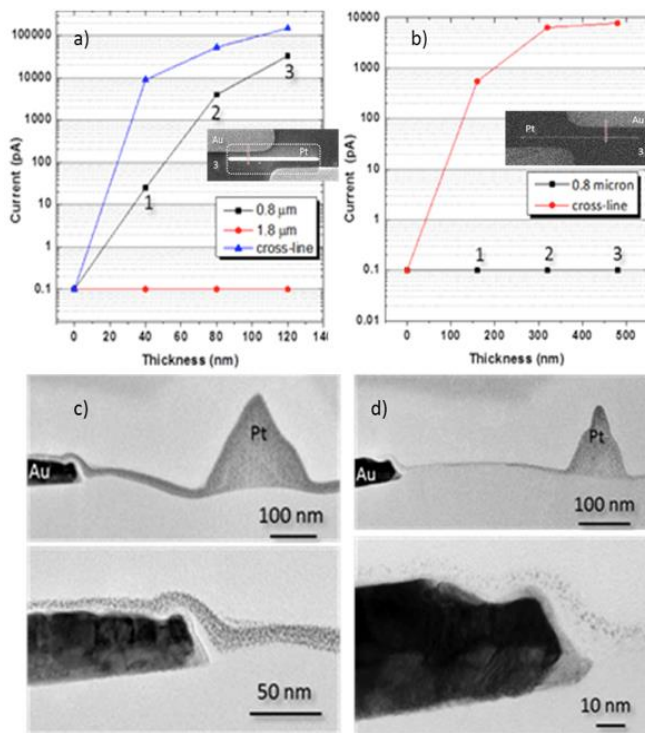


Figure 3. Plots of current vs nominal thickness of the deposits measured by in situ EBID/electrical testing for various devices developed at a) 5 kV and b) 30 kV. c) and d) are corresponding cross-section TEM images at two different magnifications.

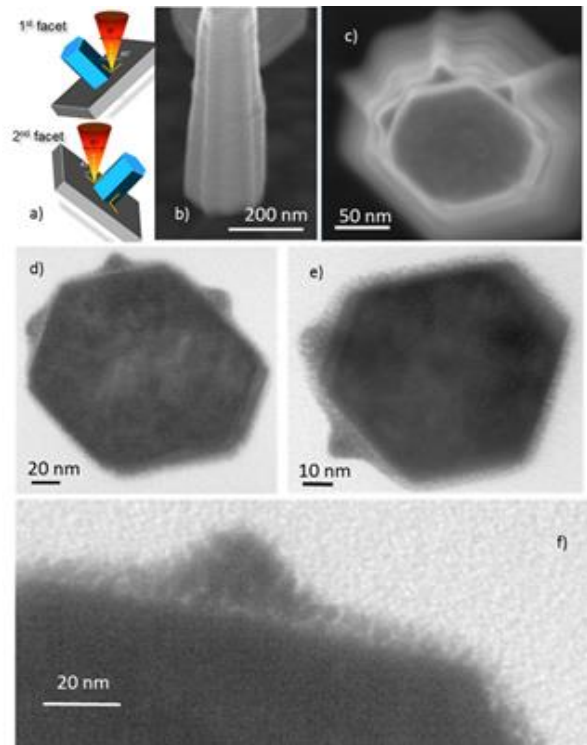


Figure 4. a) Schematics of the EBID writing geometry for ZnO pillar structures, b) and c) tilt and top down SEM views of a ZnO pillar with Pt lines written at along the whole length of 3 neighbouring facets, d) corresponding plan view TEM, e) TEM for a smaller diameter pillar and f) higher resolution TEM image from one of the facets part of the pillar shown in d).

Architecture-I devices: technical challenges and solutions

The complex, truly 3D topology of A-I configuration calls for a *direct-write* technique that ensures desired flexibility and controllability at the sub-micron scale. 3D printing or laser metal writing can be used to directly write metal interconnect lines. Unfortunately, obtained structures are limited to the micron scale. Scanning probe lithography techniques such as thermal or dip-pen nanolithography has already been used to directly write metal line structures with nm resolution. However, a major limitation to these techniques is in the inability to pattern onto vertical surfaces and to easily find/navigate around already existing arrays. *Electron beam induced deposition* (EBID) using focused electron beam and flow of organometallic precursors, brought in the near vicinity by a gas-injector system (GIS), can overcome these limitations. EBID is a very versatile and flexible direct-write method that has been extensively used for prototyping planar NW devices and devices based on 2D materials². However, until now, EBID has not been applied in developing electrically insulated contact lines along the length of individual facets of vertical structures. The case of EBID on the facets of sub-micron vertical crystals would be even more complicated as the support is not planar. Scattered electrons can leave the crystal through the neighbouring facets (such are absent when writing on planar supports) as well as through the growing deposit and cause “halo” deposition *i.e.* deposition outside the nominal dimensions of

² Tham, D.; Nam, C-Y.; Fischer, J. E.; Microstructure and Composition of Focused-Ion-Beam-Deposited Pt Contacts to GaN Nanowires. Adv. Mater. 2006, 18, 290–294.

the contact line creating electrical shorts between the contact lines.³ Thus, the main aims in achieving *Architecture I* devices can be formulated in the following way:

- to find EBID conditions for electrically insulated lines with close proximity on planar substrates;
- to demonstrate EBID process flow for contacting ZnO NW vertical facets;
- to determine structural and electrical properties of contacted ZnO NWs devices;
- to measure an electrical response from a single wire facet under applied mechanical stress.

Nano deposition of the electrodes

In order to estimate the contribution of the “halo” deposition in forming electrically insulated EBID lines, the Pt lines were written in parallel to two pre-defined Au electrodes separated by varying distance (0.8 – 10 μm) (see insets in Fig. 3). Using SEM probing capabilities, the current measurements were taken sequentially, i.e. a pre-set minimum deposition step was chosen and repeated, whereby the current at 20 V between the electrodes was recorded after every consecutive deposition step. For comparison, Pt-lines directly linking the Au electrodes (cross-line) were developed and measured using the same procedure. We have investigated depositions at two incident beam energies of 5 and 30 kV (Fig. 3a&b), at optimal deposition parameters (single pixel lines, dwell-time, beam current, etc.) following our previous report.⁴ Additionally, Pt ion-beam induced depositions (IBID) were accomplished following the same procedure of sequential deposition and recordings of the current between the Au electrodes. As shown in Fig. 3c&d, by converging obtained *in situ* electrical data and post-factum cross-sectional TEM imaging of the structures, we demonstrated the clear advantages of using EBID at high (30 kV) incident energy for minimized “halo” deposition and electrically insulated structures at sub-micron proximity (down to 800 nm separation).

The “halo”-optimization step has been followed by development of EBID process suitable for contacting vertical facets of ZnO NWs. The EBID were performed at 30 kV after tilting the stage of the instrument so that the surface of the ZnO facets is at 45 degrees to the incident beam (Fig. 4a). Writing on neighbouring or diametrically opposite facets was accomplished after rotating the stage and aligning the beam to the corresponding tilted ZnO facet. The top-down SEM image shows that at 30 kV the lines were well-centred along the width of the facets, demonstrating good stability during the deposition process. Contrary, any attempt to write structures at low incident energy (5 kV) resulted in highly misaligned structures due to the increased sample drift, caused most probably by a sample surface charging. Despite of the successful device fabrication, the performed experiments also show that the main drawback of the EBID direct write process is its very low productivity and very complex conditions to execute (over 3 hrs per wire device). Hence, it is extremely challenging for automation and for high throughput device integration in CMOS compatible environment.

Structural and electrical properties of contacted ZnO NW devices.

The TEM images allowed us to determine not only the accurate shape and structure of the Pt-lines but also to observe the “halo” deposition on the ZnO facets. Most importantly, the shape of the Pt-lines is Gaussian like as expected. The data suggests that at the corners of the facets the continuity of the “halo” layer is affected, hence, benefiting the formation of electrically insulated lines (Fig. 4d). For comparison, Fig. 4e shows a TEM image taken at another NW having smaller diameter. As for the writing Pt lines the same parameters were used, formed “halo” layer is at about 6-7 nm in thickness decreasing towards the corners of the facets.

³ Plank, H.; Smith, D. A.; Haber, T.; Rack, Philip D.; Hofer, F. Fundamental Proximity Effects in Focused Electron Beam Induced Deposition. *ACS Nano*, 2012, 6, 286-294.

⁴ O'Regan, C.; Lee, A.; Holmes, J. D.; Trompenaars, P.; Mulders H.; Pektov, N.; Electrical properties of platinum interconnects deposited by electron beam induced deposition of the carbon-free precursor, Pt(PF₃)₄, *J. Vac. Sci. Tech. B*, 2013, 31, 021807.

However, due to the smaller width of the facets (30 – 60 nm, in comparison to 60 – 100 nm for the first pillar), the “halo” layer at the corners did not appear discontinuous.

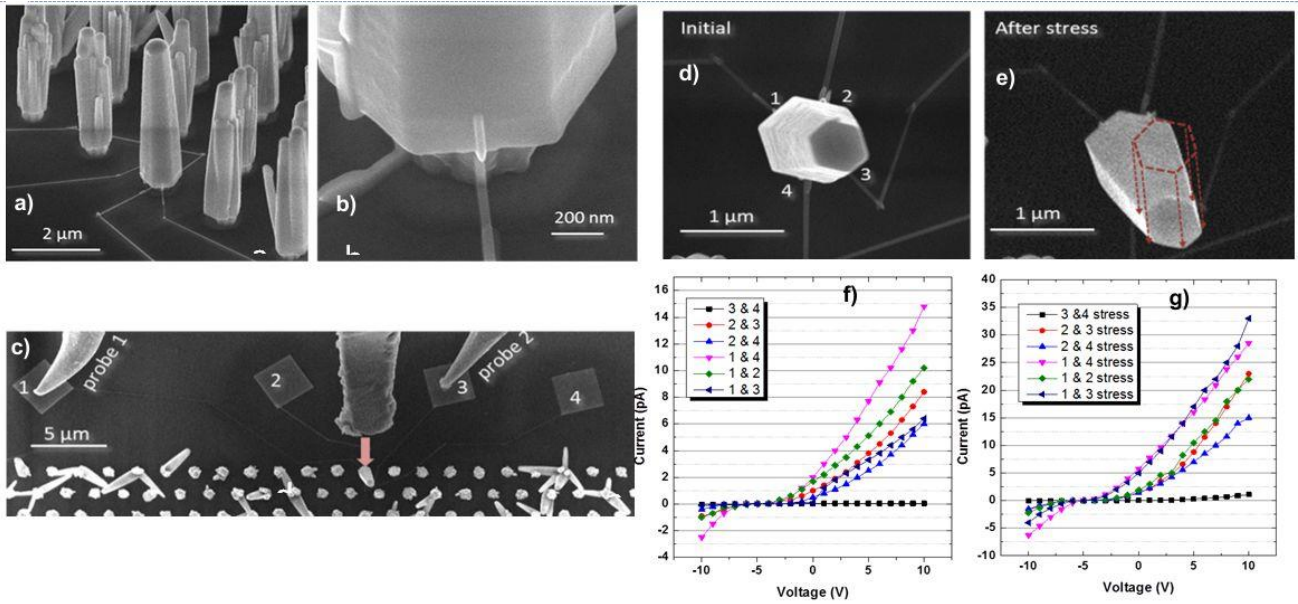


Figure 5. a) and b) tilt view SEM images of a ZnO pillar device featuring, c) top down view of the whole circuitry and corresponding SEM images d) before and e) after applied stress, and associated current/voltage curves f) before and g) after applied stress.

To confirm that the fabricated Pt-lines were indeed electrically insulated, the A-I devices with deposited line contacts on ZnO pillar facets connected to the corresponding contact pads were processed by EBID at 30 kV. Fig. 5a-d show the SEM images of such device, whereby four diametrically opposite facets were contacted (see Fig. 5d for the facet enumeration). Using *in situ* electrical nano-probes, two terminal current-voltage curves were obtained for various pairs of facets (Fig. 5f). The curves were characteristic for non-symmetric rectifying (diode-type) devices. If we assume that there is no build-in potential due to the piezoelectric effect, the rectifying behaviour can be explained by two back-to-back Schottky diodes with significantly different barrier heights.⁵ During the experiments, it was confirmed that the contact lines were structurally and electrically insulated for NWs with cross sections down to 150 nm. Developing insulated lines by EBID for the NWs having smaller diameter is very challenging.

At the final step, in order to obtain data on the electro-mechanical properties of the NWs, an additional mechanically driven nano-probe was employed to apply *in situ* stress to the ZnO NW. Fig. 5e shows the resulting NW constant deflection from its original position. This deflection is caused by one-directional inclination of the NW hexagonal body, and shows no delamination from the base of the NW. The resultant tilt is about 5 degrees from the initial orientation of the NW. Neither NW bending nor rotation along its axis was observed. The current-voltage data was recorded after stress application on the same pairs of facets (see Fig. 5g). The overall shape of the curves was preserved for all facet pairs indicating that the contact lines have not degraded after the mechanical impact. The interesting finding is that the current values at positive potential for all facet pairs have increased by 2-5 times in comparisons to those measured before applying stress. We suggest that the applied stress resulted in an increased build-in potential inducing a more effective charge separation at the opposite facet.

⁵ Lu, Y.; Brillson, L. J. ZnO Schottky contacts and barriers. *Appl. Phys. Rev.* 2011, 109, 121301.

Positioning Architecture 1 within PiezoMAT

Architecture 1 is at the proof-of-principle level (“high risk – high ambition”) aiming at achieving prototype devices and accepting low productivity for fabrication. While it supplied important data in terms of understanding single ZnO NW behaviour, it certainly posed numerous problems in terms of repeatability, ease of use and throughput. On the positive side, even at a very early stage of the project, studies of A-I devices have increased the awareness of the upcoming difficulties/challenges in terms of complexity and operation principle (e.g. piezoelectric vs semiconducting properties which in principle are inherently coupled in ZnO nano-devices). Finally, A-I related research was truly cooperative undertaking requesting contributions of nearly all consortium partners.

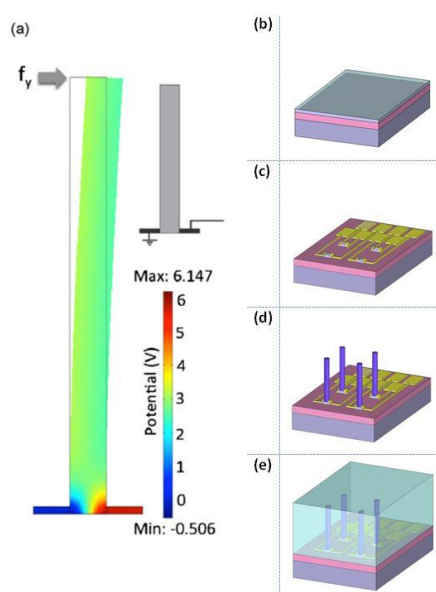


Figure 6. a) piezo-potential distribution along the NW upon bending.⁶ b)-e) Main stages of the fabrication process carried out by the consortium partners and detailed in the following chapters: seed layer deposition by PLD (a), circuit process (b), NW growth (c), and polymer encapsulation of the sensor array (d).

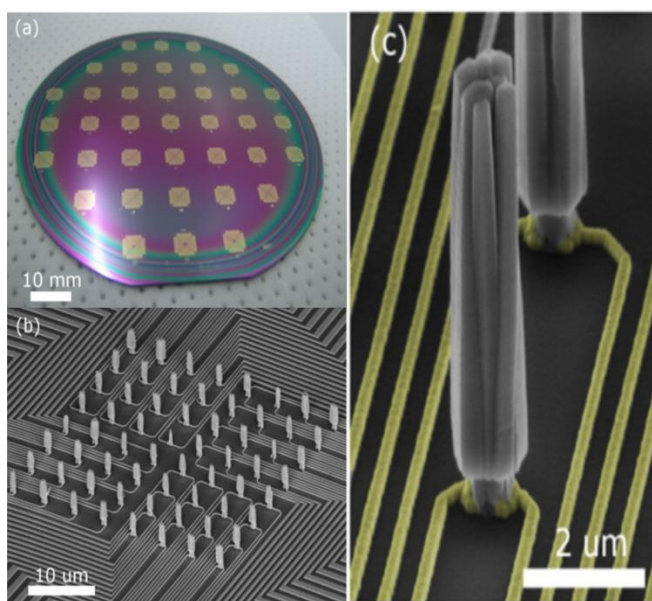


Figure 7. On-chip integrated piezoelectric NWs. Photo of Si wafer with 37 NW chips (a); SEM image of the 8x8 NW array (b), ZnO NW pixel contacted by a pair of bottom electrodes (Ti/Au) colored in yellow (c).

3.3 Architecture II: bottom-bottom contacted nanowires

Though the principle of the sensor operation and corresponding finite element method (FEM) analysis were reported by Falconi et al.,⁶ a functional NW-based bending force sensor with the bottom-bottom contact configuration (A-II) has not been demonstrated yet. According to the FEM simulations, the maximal piezo-potential gradient is concentrated near to the root of the NW (Fig. 6a), which is to be exploited by this device architecture. It should be noted that, in this study, the main objective for electromechanical characterizations was to quantify changes in external current flowing through a NW (under a constant bias). This is due to the

⁶ reprinted from Falconi et al., Sens. Actuator B. 2009, 139, 511

fact that after NW deformation, the current is modulated either by the strain-induced piezo-charges or by the Schottky barrier height variation, which is governed by the deformation potential of ZnO. This approach was selected instead of the direct measurement of the fixed piezo-charges, due to the extremely low capacitance of the bottom electrodes, which implies that the latter measurements would be highly challenging or even impossible for the considered device configuration. In contrast, the ZnO NW was electrically tested as a mechanically-gated transistor, where strain-dependent piezoelectric polarization acts as a gate-controlling signal that modulates the external current passing through the device, thereby providing a more robust sensor signal.

The main stages of the fabrication process for A-II sensor chip on Si wafers are shown schematically in Fig. 6b-e. First, high-quality ZnO seed layers were deposited onto a 3" SiO₂ coated Si wafer (Fig. 6b). The deposition was followed by the realization of matrix circuits with a dimension of 8x8 (Fig. 6c). NWs were wet-chemically grown onto the remaining ZnO seed islands between the pair of the bottom metal contacts (Fig. 6d). Cross-linked polymer with tailored properties was used to encapsulate the NW arrays in the last stage (Fig. 6e).

Seed layer deposition using PLD

For the deposition of ZnO seed layers on the A-II chips, *pulsed laser deposition* (PLD) technique was used. In doing so a ZnO target was irradiated by a focused pulsed laser beam of a KrF laser beam. The high energy transfer from the laser beam into the target leads to an ablation of the target material and plasma is formed. This plasma propagates to a substrate, which is mounted vis-à-vis to the target. The propagation of the plasma can be controlled by the background partial pressure. A high pressure leads to a large scattering of the plasma with the atoms of the background gas so that the main particles of the plasma will not reach the substrate. In contrast, too low background pressure leads to a high momentum of the plasma at the substrate. As a result, the plasma species are poorly deposited on the substrate and a "re-sputtering" of the already deposited particles can occur. Other important tuning parameters are the temperature of the substrate, and an precise balance between diffusion (responsible for smooth and homogeneous films) and desorption of the arrived particles from the plasma.

Typically, 10×10 mm² substrates are used in PLD process. However, for the compatibility with the subsequent process steps, homogeneous seed layers on 3" wafers are essential. This is quite challenging for PLD, mostly, due to the inhomogeneous particle density distribution in the plasma plume. In order to reach a homogeneous film on 3" substrates, the off-axis PLD technique is used. In this case, the substrate and the target are aligned in such way, that the centre of the target is not in-line with the centre of the target, and therefore, not with the centre of the plasma plume. A rotation of the substrates during the deposition process reduces the impact of the inhomogeneous particle density distribution of the plasma plume on the substrate.

In the deposition experiments, two types of substrates are used: c-plane oriented sapphire (for the test purposes) and conventional 3" silicon wafer with a 1 μm thick thermal SiO₂ film. The first type ensures a high crystalline quality of the ZnO seed layer, and thus, supports the growth of single-crystalline NW of the highest quality. The use of Si wafer leads to a slightly reduced crystalline quality of the seed layer (and consequently, to a lower quality of the NW pixel), but ensures the compatibility with the standard Si processing. For both wafers, the deposition process was optimized, and the optimum deposition temperature and oxygen partial pressure was found to be about 750°C and 0.002 mbar, respectively. In order to ensure a high resistivity of the seed layer, which is desired for the better performance of the A-II chips, the ZnO target was doped with 0.25 wt % of Mg. It reduces a free charge carrier concentration effectively due the self-compensation effect. In doing so high-quality Mg:ZnO seed layer series with predefined thicknesses of 50 nm and 100 nm were fabricated. The homogeneity of the film thickness of ~ 5% is revealed by spectroscopic ellipsometry mapping over the entire wafer. The specific resistivity is determined on a reference sample grown on 10×10 mm² c-plane sapphire substrate to be 2×10⁴ Ω·cm, with the carrier concentration being below 10¹⁵ cm⁻³.

Chip processing and NW growth

Due to the complex, 3D structure of A-II chips, the fabrication process flow consists of more than 25 technological steps, including five electron beam lithography (EBL) alignments. First, ZnO islands were patterned using Ar reactive ion etching. They were contacted by Ti/Au metal lines from two sides, and finally the growth of the NWs were carried out in sub-micron sized nucleation windows using a *wet chemical growth method*. The fabrication process had several challenges to be solved, i.e. accurate (< 50 nm) alignment of the EBL patterns, high-quality metal lift-off process after EBL and photolithography, removal of sample charging during EBL, mesa etching of ZnO seed layer along with protection of ZnO mesa island against unwanted etchings. The processed 3" Si wafer holds 37 chips (Fig. 7a). Each of them has an active sensor array of 8x8 individually contacted NWs located in the chip centre (Fig. 7b). The inter-pixel distance of 5 µm corresponds to a very high lateral resolution of 5080 dpi. Due to high quality of ZnO seed layer, the deposited ZnO NWs show an excellent c-axis orientation even being grown on amorphous, SiO₂ covered Si surface. Nevertheless, the ZnO pixels grown on Si templates are multi-NW objects (multi-core, Fig. 7c), in contrast to single-NW pixels grown on epitaxial ZnO/sapphire substrates (not shown here). High resolution SEM images show that the NW pixels were positioned precisely onto the read-out contacts with an accuracy < 50 nm throughout the whole 3" wafer (Fig. 7c).

Encapsulation of A-II chips

ZnO NWs cannot undergo direct contact with the finger, therefore a polymeric encapsulating layer is required in order (i) to provide physical protection of the NWs, and (ii) to transfer the force from finger to the NWs more efficiently. To ensure sensor robustness, the polymeric layer should also exhibit appropriate chemical inertness along with water- and oil-repellence. To achieve these properties, novel formulations of UV-cross-linkable polymeric materials were developed, prepared and deposited as thin layers on the NWs using spin-coating by following the recommendations derived from FEM simulations (Fig. 8).

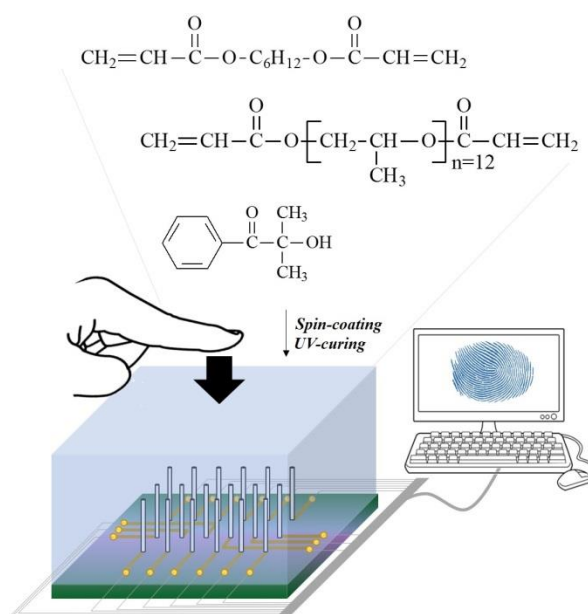


Figure 8. UV-cross-linkable polymeric material for NWs encapsulation.

An important part of the work was first dedicated to the selection of the most suitable polymeric formulation in terms of viscosity and mechanical properties (i.e. the Young's modulus). A multi-component,

solvent-free, spin-coatable, and UV-cross-linkable polymeric material was finally retained here. The spin-coating process was selected since: (i) a liquid deposition system must ensure the encapsulating material to be well-spread over the sample, particularly in the vicinity of the NWs and (ii) it enables fine control of the encapsulating layer thickness by varying the rotation speed during spin-coating. The UV-curing, which is an efficient and environmentally friendly process commonly used in microelectronics industry, was chosen because it leads to the crosslinked and thus chemically inert material. The UV-crosslinked material based on 1,6 hexanediol diacrylate (HdA) and poly(propylene glycol) diacrylate (PPGdA) was finally selected.

In the case of A-II sensors, the NWs should be fully covered by the encapsulation layer since the piezoelectric signal is collected at the NWs “foot”. Moreover, the recommended parameters from COMSOL Multiphysics 2D FEM model for the targeted near-optimal values of polymer Young’s modulus (mechanical properties) and cap height (thickness of the polymer layer above the NWs) were within the range of 0.1-0.4 GPa and 2-4 μm , respectively. To meet these recommendations, the formulation containing 40 wt% of PPGdA and 60 wt% of HdA was implemented. Indeed, this formulation led to the encapsulation layer exhibiting the most favourable compromise between the targeted mechanical properties ($E^* = 0.12$ GPa) and formulation viscosity (25 cP), thereby enabling spin coating processing.

After the polymer development step, functional A-II chips were encapsulated with the selected formulation using spin-coating/UV-curing process, and it was figured out that the encapsulation layer thickness is greatly affected by the properties of wafer surface (i.e. its chemical nature, quality, morphology, presence of contact lines, etc.). During the following experiments, an additional step, Al_2O_3 coating, was developed, which provides more homogeneous polymer thickness distribution.

Finally, it must be mentioned here that the surface properties (hydrophobicity and lipophobicity) of the encapsulation materials were proved to be enhanced by the introduction of fluorinated acrylate compounds. Indeed, hydrophobicity is of great interest here since electronic devices are very sensitive to ambient water vapour and oxygen gases, which induce corrosion effects, film delamination and may ultimately lead to premature failure. Lipophobicity is also a major property that must be reached since the device will be repeatedly expose to fingers grease and other external stresses.

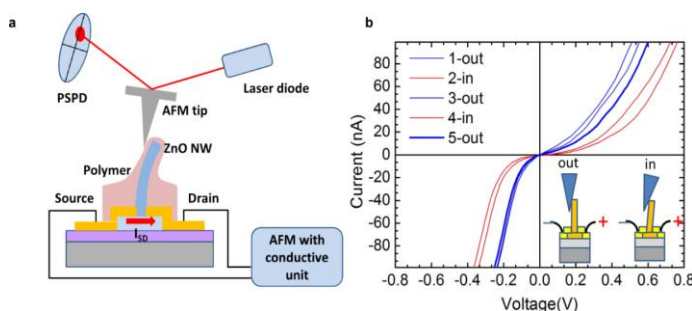


Figure 9. Schematic of the AFM-based NW bending setup (a) and current-voltage curves taken at subsequent loading cycles (b). The unloaded and loaded curves indicated an acceptable degree of reproducibility.

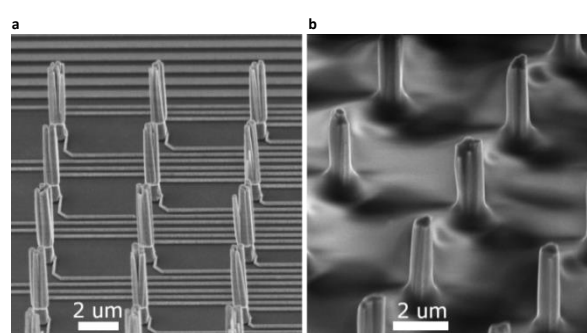


Figure 10. SEM images of ZnO NWs (a) before polymer encapsulation and (b) after encapsulation.

Electromechanical and structural characterization of the A-II chips

Static electromechanical tests of the contacted and polymer-coated NWs were carried out in an AFM-based measurement setup by means of the simultaneous monitoring of the lateral force signal and source-drain current as depicted in Fig. 9a. Prior to the actual measurement, the lateral force signal of the AFM

probe/instrument system was calibrated by a vertically mounted contact mode AFM tip having a known flexural spring constant (k_n).

It was found that as-grown NWs without polymer protection fracture easily during the test. On the other hand, with polymer coating (Fig. 10b) the NWs withstood several bending cycles with a maximum lateral force of about 2 μN without any fracture event. Moreover, as shown in Fig. 9a, a significant and fairly reproducible change of the non-linear current-voltage characteristic was recorded under the influence of the lateral load ($F_l = 1.1 \mu\text{N}$), which validates the force sensing capability of the polymer-surrounded ZnO NW.

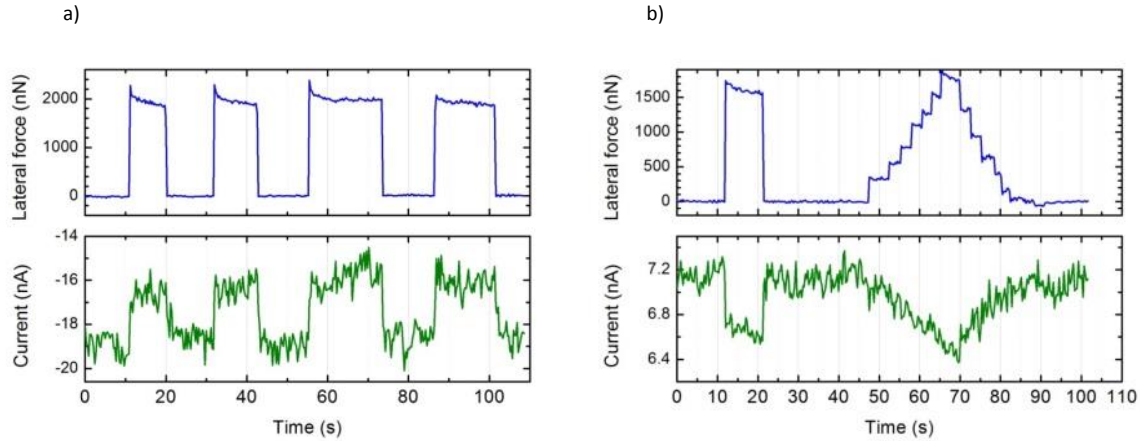


Figure 11. Time-domain lateral force and current signal monitoring at periodic bending (a) and at loading with arbitrary profile (b). The bias voltages were 0.2 and 0.5 V, respectively. The active NW pixels are highly sensitive to the lateral bending load.

Time-domain current monitoring of the same NW pixel upon various lateral force loading schemes are shown in Fig. 11a&b. Current modulation reproduces the shape of the lateral force modulation, which bodes well for grey scale finger print sensing, i.e. instead of the binary information (relaxed or bent) we are able to collect electrical data which are proportional to the magnitude of the lateral bending force.

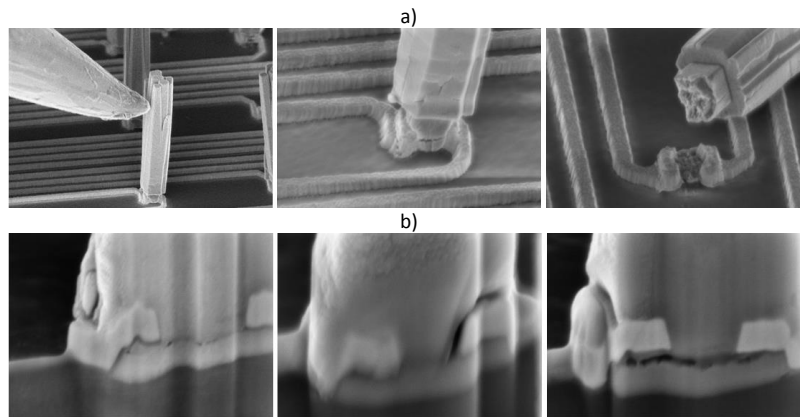


Figure 12. a) Bending of the ZnO crystals using a SEM micromanipulator. Fracture takes place at the ZnO seed island / hydrothermal ZnO interface. b) Micro-cracks and voids around the threefold junction of ZnO seed layer, hydrothermal ZnO, and metal (Ti/Au) contact which can be attributed to the limited bending strength and electromechanical insensitivity.

Though the obtained signals correspond to an extremely high gauge factor, the major part of the NWs was found to be inactive. Hence, lateral force mapping using the sensor matrix demonstrator of 8x8 pixels is still missing. By comparing the current-voltage curves of the pixels the difference between active and inactive

pixels was not obvious. One possible explanation of the insensitivity is the plastic deformation or even fracture of the NWs upon bending. In order to reveal the origin of the limited bending strength bending tests using an SEM micromanipulator were carried out on 16 NW pixels. It was found that the fracture occurs always along the NW/island interface (Fig. 12a). The interface quality at the bottom of three inactive NW pixels was observed in SEM using FIB cut technique. As shown in the Fig. 12b each NW shows a slightly different interface structure but a crack or void-rich region can be found at the interface for all NWs. It is very likely the origin of the limited bending strength.

In summary the first experimental demonstration of a bottom-bottom contacted type NW based tactile sensor (Architecture II) was realized in the PiezoMat project. The developed fabrication process was carried out on 3" Si wafer which was covered by highly c-axis oriented PLD ZnO. The optimized procedure consists of several nanolithography steps with sub-50 nm lateral accuracy, a wet chemical growth steps for the bottom-up synthesis of the piezoelectric transducers, and polymer encapsulation using specific cross-linked polymer. Active pixels show high sensitivity against micro-Newton ranged lateral forces and very high gauge factors. Nevertheless, it was also found that the major part of the NWs in the 8x8 array is inactive which can be attributed to the microcracks observed at the root of the ZnO crystals. Because of the limited strength and low reproducibility of the active pixels the consortium focussed more deeply in the mechanically more robust top-bottom contacted architecture (A-III). Bottom-bottom contacted type tactile sensor may triggers new applications in the fields where the detection of the lateral component of the micro-Newton range forces is required (e.g. traction force of living cells).

Multiphysics FEM modelling of the bottom-bottom contacted ZnO NWs for bending force sensing

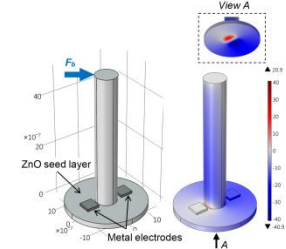
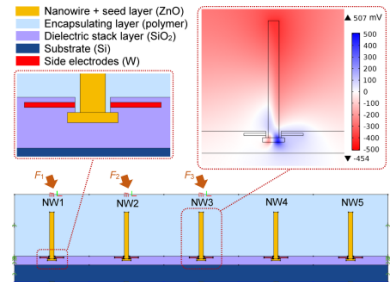
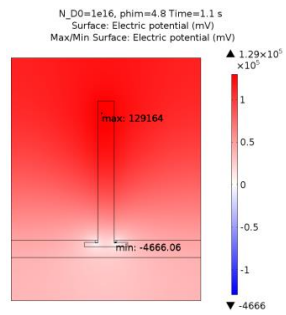
Numerical and analytical modelling activities were pursued in the project with the objectives to provide useful inputs during sensor design workflow and to gain deeper understanding about the electro-mechanical behaviour of the dynamically deformed ZnO NWs. A wide range of multi-physics finite element method (FEM) models of single and arrayed vertical ZnO NWs were implemented during these studies using COMSOL Multiphysics® software (see Table 1). The NWs were modelled as individually-addressable pressure sensing pixels by connecting them to separate external capacitors, which represented the readout circuitry of the sensor. From a mechanical point of view, the models were treated as quasi-static, while electrically – as dynamic. To deform the NWs, ramping and semi-harmonic loads were used to imitate the actual pressing with a finger and time-dependent numerical studies were performed to predict voltage, charge and current signals generated by each NW.

Different versions of FEM models, characterized by varying degree of structural, electrical, physical and dimensional complexity, were successfully implemented: starting from a classical piezoelectric model of a single NW to the encapsulated fully-coupled piezoelectric-semiconducting-circuit multi-NW model. For example, the structural configuration of the most complex “chip-based” piezo-semi-conductive model (e.g. ver. FEM2.3) corresponds to the chip layout that was developed in the project. Availability of different model versions allowed avoiding computationally-prohibitive simulations and rationally addresses modelling challenges associated with the solution convergence of time-dependent multi-physics simulations, particularly in the case of piezo-semi-conductive models with nonlinear Schottky contacts or models of the encapsulated NW array with nonlinear contact-based mechanical interactions imposed on multiple NW/polymer interfaces. Therefore, availability of different model versions allowed effective and efficient tackling of specific computationally-intensive simulation tasks by ensuring reasonable solution times and consistent numerical convergence.

The developed models are classified into two large groups in terms of the modelled sensor “Architecture”, which is characterized by a distinct contacting option (i.e. electrode topology used for charge collection). In

this section, A-II bottom-bottom contacting option with side electrodes that are positioned at the root of NW for bending force sensing is considered. The side electrodes may be either separated from the NW (suspended) or they may be contacted to it. Extensive parametric numerical studies were conducted with different model versions, which enabled prediction of electro-mechanical responses of the NWs under different mechanical loading conditions and input system parameters (e.g. NW morphologies, electrode topologies, structural chip configurations, material properties, external circuit capacitances, etc.).

Table 1: Summary of the implemented FEM models for A-II

Version No.	Type of model	Main features	Model images
FEM2.1	Single-NW piezoelectric model (3D)	<ul style="list-style-type: none"> ▪ Idealized structural & electrical configuration (classical piezoelectric theory): <ul style="list-style-type: none"> - ZnO: dielectric. - Electrical contacts: ohmic. - Electrical properties of all dielectric and conducting stack layers accounted for. ▪ No encapsulation. 	
FEM2.2	Encapsulated multi-NW piezoelectric chip-based model (2D)	<ul style="list-style-type: none"> ▪ Realistic structural configuration: NWs integrated on a multi-layer chip stack & encapsulated in a polymer. ▪ Idealized electrical & physical configuration: <ul style="list-style-type: none"> - ZnO: dielectric. - Electrical contacts: ohmic. - Electrical properties of all dielectric and conducting stack layers accounted for. 	
FEM2.3	Encapsulated single-NW piezo-semiconductive chip-based model (2D) /directly extendable to NW array/	<ul style="list-style-type: none"> ▪ Realistic structural configuration: NWs integrated on a multi-layer chip stack and encapsulated in a polymer. ▪ Realistic electrical & physical configuration: <ul style="list-style-type: none"> - Coupled piezoelectric & semiconducting properties in ZnO. - Electrical contacts: ohmic or Schottky (nonlinear) - Electrical properties of all stack layers accounted for. 	

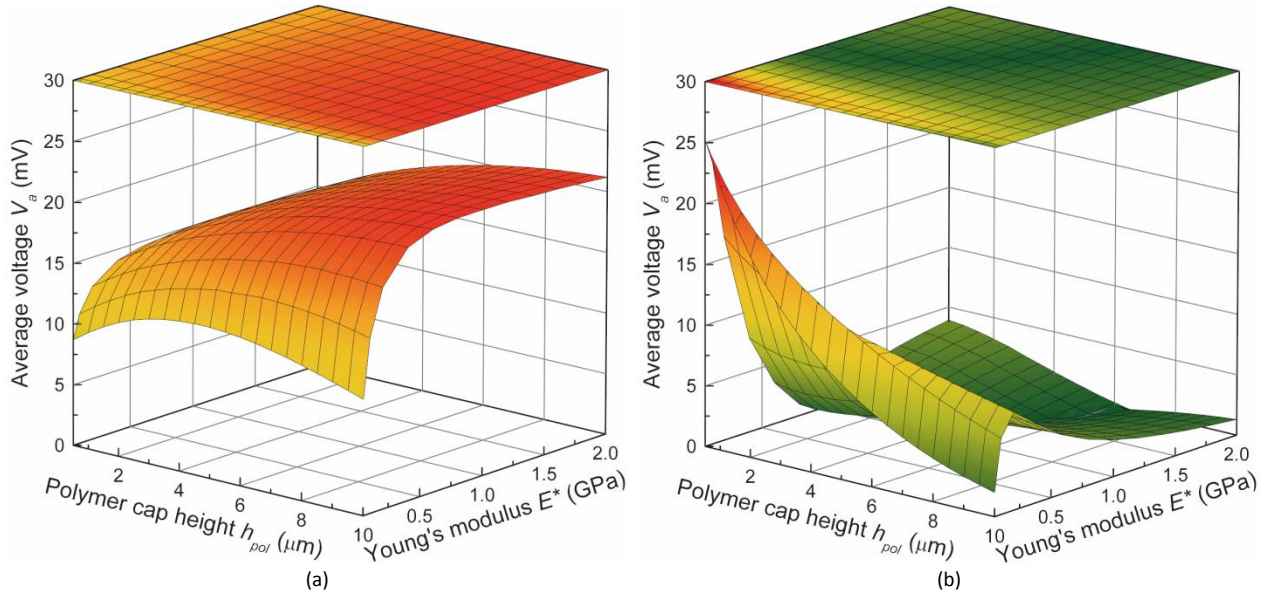


Figure 13. Representative simulation results obtained with the encapsulated multi-NW piezoelectric model (FEM2.2): surface plots of average voltage signal generated by the directly loaded NWs as a function of polymer cap height and Young's modulus for the case of pure vertical load of $F_v = 1$ MPa (a) and oblique load of $F_h = F_v = 1$ MPa (b). Model properties: NW width – $0.5 \mu\text{m}$, NW length – $15 \mu\text{m}$, inter-NW spacing – $8 \mu\text{m}$, external capacitor connected to NW – 10 fF .

Main results of the numerical studies for Architecture II can be summarized as follows:

- Using the single-NW piezoelectric 3D model (ver. FEM2.1):
 - Strain-induced piezoelectric charge signal is negligible (several electrons released) for pressure loads that are expected in actual sensor usage ($\sim 2 - 50 \text{ kPa}$). Exploitable strain-induced signal from the single NW is predicted only when the load reaches several MPa;
 - NW under bending generates $>10^3$ larger voltage at the expense of charge signal, which is reduced 3 times in comparison to the A-III NW under compression;
 - Higher aspect ratio NW is strongly advantageous in terms of voltage and current signal, though charge increase is insignificant (pure bending case);
 - The combined bending and compression of the NW (expected during the actual sensor usage) is favourable in terms of charge signal, but complicates voltage signal in time-domain;
 - Addition of the dielectric top layer over the seed layer as well as thickening of the seed and top layers leads to the reduction of electrical signals;
 - Separation of the side electrodes from the NW leads to reduction of the electrical signals with respect to the case of electrodes that are fully contacted to the NW;
- Using the encapsulated multi-NW piezoelectric chip-based 2D model (ver. FEM2.2):
 - The most rational (near-optimal) values of Young's modulus and thickness of the encapsulating polymer layer were established in order to maximize electrical signals generated by the piezoelectric NWs, which would facilitate the detection and post-processing of the signals;
 - The average piezoelectric signals exhibit more complex variation with changing polymer Young's modulus and cap height when horizontal load component is present and when NW aspect ratio is increased (Fig. 13)
- Using the encapsulated single-NW piezo-semiconductive chip-based model (ver. FEM2.3):
 - In low-load range (roughly: $<1 \text{ MPa}$), the electrical signals: a) have relatively high magnitude that cannot be attributed to the strain-induced piezoelectric effect, b) are insensitive to the increasing

bending force. In high-load range (roughly: $>1 - 2$ MPa) the charge and voltage signals are very weakly sensitive to the increasing load (current is not sensitive)

- Magnitude of electrical signals strongly depends on the maximum donor doping (n-type) concentration in ZnO: the most pronounced increase is predicted in the range of $10^{18} - 10^{19} \text{ 1/cm}^3$. Current signal at 10^{18} cm^{-3} is on the order of several nA, which is in agreement with the in-situ current measurements performed on the polymer-coated A-II NWs.

In addition, analytical models of an ideal vertically-aligned ZnO NW under pure compression and bending were derived on the basis of sound physical principles and were used to validate the accuracy of the single-NW piezoelectric FEM models (the models agree within 3%). Modelling results were correlated to the findings of the AFM-based electro-mechanical characterizations performed on the stand-alone non encapsulated ZnO NWs and the measured high-magnitude electrical signals were explained by the proposed analytical model of spontaneous polarization charge.

3.4 Architecture III: top-bottom contacted nanowires

Si carrier-chip fabrication

The Architecture III (A-III) is a top-bottom contacted NW configuration, which is shown schematically in Fig. 13b. The developed chip is a matrix with dimensions of 25×10 pixels featuring 1000 dpi 2D resolution, which exceeds by factor of two the main-stream fingerprint sensor.

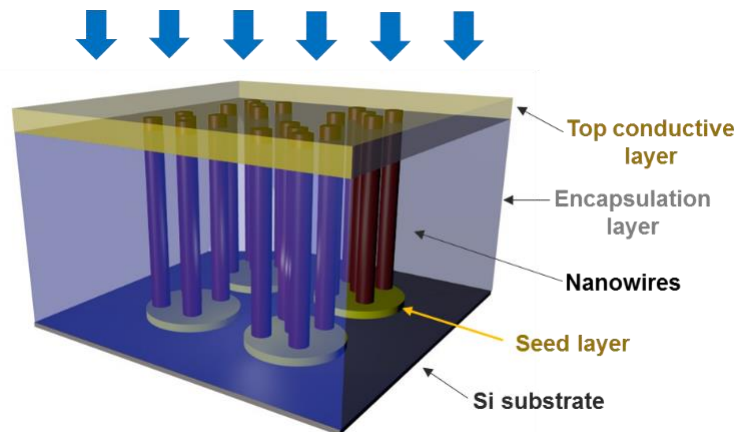


Figure 13b. Schematic view of the top-bottom contacted NW configuration (A-III)

For the final test of A-III sensor, 200 mm thick silicon wafers (100) oriented were processed in the CEA clean-room. Each processed wafer holds 43 chips with an active array of 25×10 individually contacted NW pixels located in the centre of the chip. The process flow consist of 5 main technological “bricks” for a total of around 80 process steps (including wafers identification step, SEM characterisation, FIB, optical microscope, thickness measurements, decontamination, electrical test, grinding, dicing).

- Brick I : seed layer deposition and patterning
- Brick II : tungsten deposition and electrical path patterning
- Brick III: passivation layer deposition and patterning

- Brick IV: metal deposition and contact pad patterning
- Brick V: passivation opening above seed layer for future NW's location etching of SiO₂ on seed layer (future NW's location)

The challenges for the process development are the high patterning density, the choice of materials (especially for the seed layer) and the integration. Schematics of cross-section and top view of the chip are represented in Fig. 14.

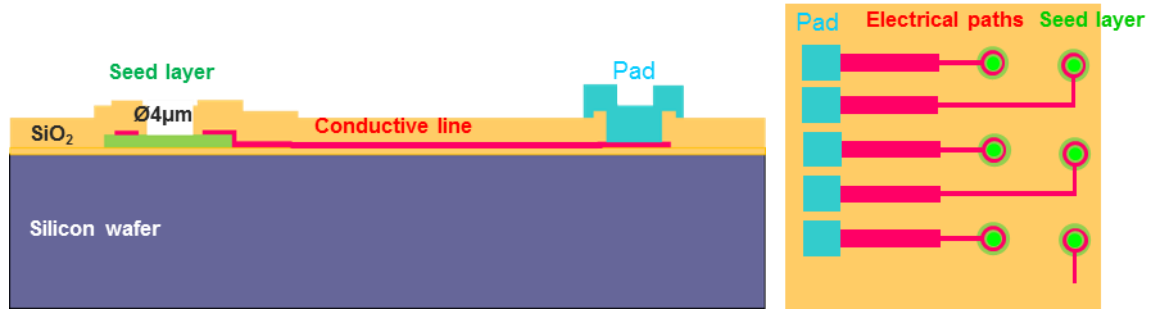


Figure 14. Schematics of one top-bottom contacted NW chip (a) cross-section (b) top view

For each chip, a high quality ZnO doped by gallium (GZO) seed layer was deposited onto silicon wafer after thermal oxidation. The seed layer was then patterned in 25x10 matrixes, which was a challenging step. Indeed, the GZO is very sensitive to humidity (corrosion issues) and is etched in almost chemical products. Therefore, only dry process are possible. The pixel diameter is 8 μm and the inter pixel distance is 15 μm which corresponds to a resolution of 1000 dpi (Fig. 15a). Each GZO pattern is then individually contacted to one contact pad in aluminium-copper by tungsten electrical paths (Fig. 15b).

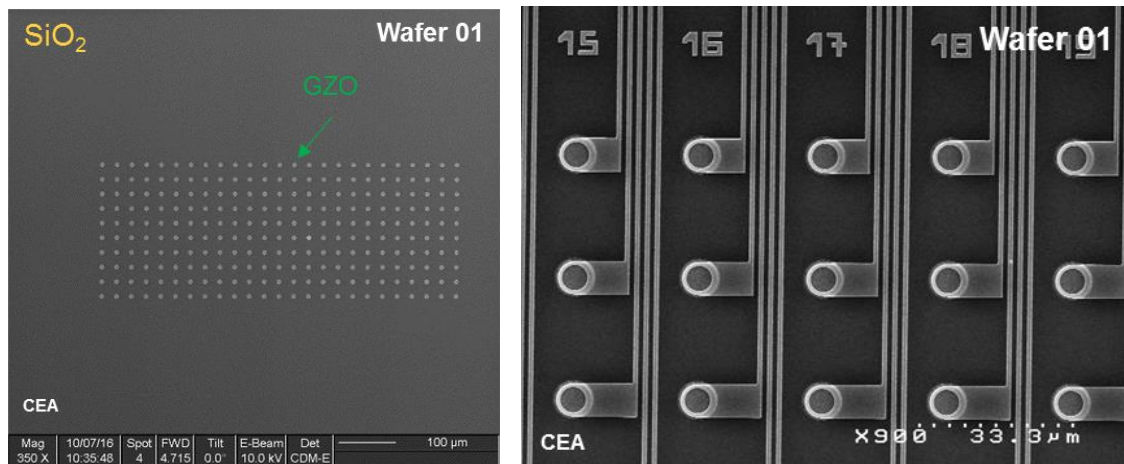


Figure 15. top-view SEM image of GZO pattern: (left) 25x10 matrix (right) one single interconnected pattern

The PECVD oxide is used as a passivation layer. This SiO₂ layer is removed only to access the tungsten contact pads and the patterned seed layer. The last opening for growth location is a critical step because of seed layer consumption during etching.

After wafer the dicing step, NW growth is performed on the chips containing 250 GZO open nucleation locations defining the future NW pixel positions (Fig. 16).

During the development for A-III chips, many technological challenges were identified and resolved by finding appropriate technical solutions. Therefore, the A-III fabrication route accumulates many technological achievements and know-hows developed specifically within PiezoMAT project such as:

- The feasibility of the technological steps in clean-room including:
 - development of a stable and reproducible process for the ZnO doped with gallium etching;
 - development of stable and reproducible process for the W etching, e.g etching of thin lines well separated;
 - development of stable and reproducible process for the final opening in the seed layer.
- Development of specific electrical tests to characterize our chips before sending to partners.
- Demonstration of feasibility of localized and contacted NWs growth on a processed 200 mm silicon wafer.

Nanowires growth on architecture III chips

The growth process was carried out on the dices comprising the following steps: i) removal of the protective resist layer from the chips; ii) PMMA spin-coating (2x500 nm) and e-beam lithography to define nucleation growth windows; iii) wet chemical growth; iv) PMMA removal and cleaning. Optical microscope image in Fig. 16 shows that the central part of the chip is almost free of parasitic NWs indicating that the cleaning step was successful.

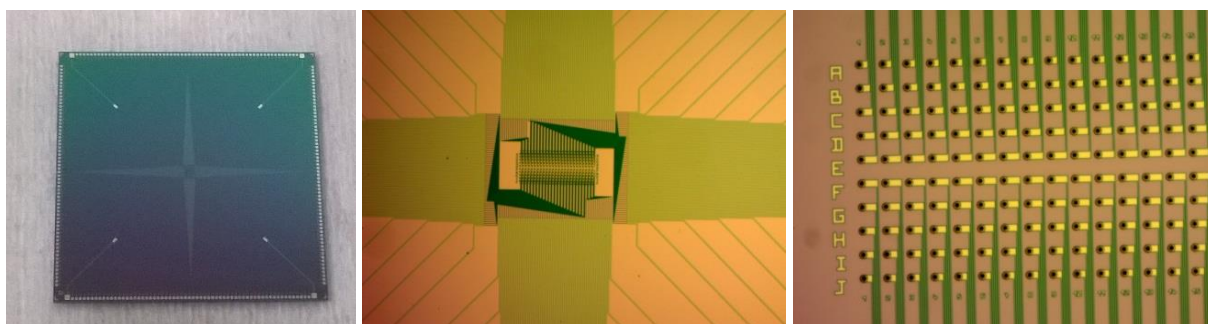
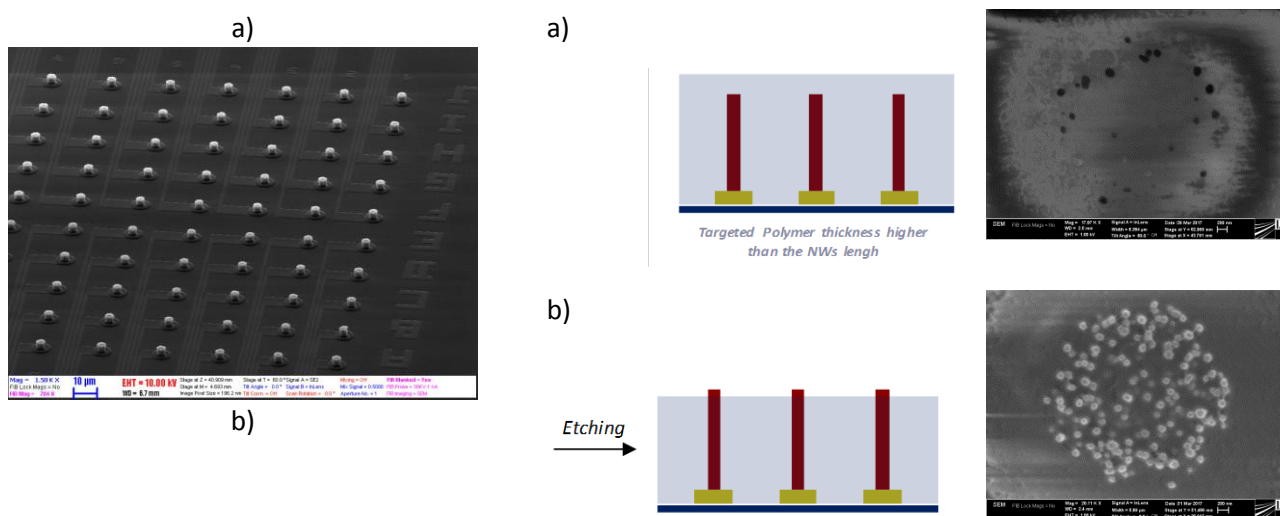


Figure 16. Optical micrograph of the (left) fully processed and diced chip (middle) central region (right) and left half of the matrix after NW growth and cleaning.



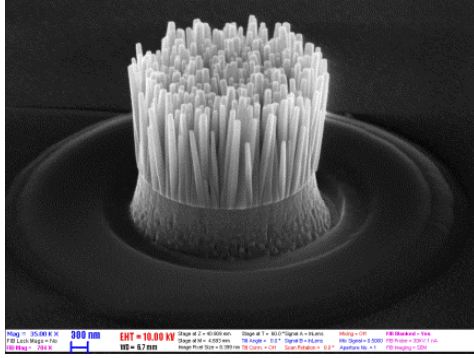


Figure 17. SEM images taken with different magnification factor showing a) A-II chip active area and b) single ZnO NW pixel after wet chemical growth through e-beam lithography patterned nucleation windows.

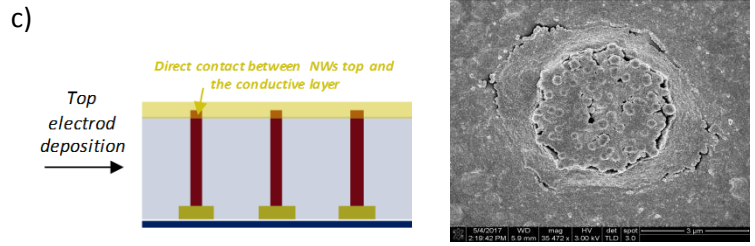


Figure 18. A-III chip encapsulation process flow: schematic representation of the process steps illustrated with plan-view SEM images of the single-pixel area (on the right side).

As shown in the SEM images in Fig. 17, the NWs are well oriented. It is partly due to the overhanging profile of the PMMA window which promotes the perpendicular NW growth and partly because of the uniaxial textured crystalline property of the GZO seed layer. The height of the NWs is approximately 3.5 μm.

Specific polymer matrix

As introduced previously for the case of A-II chips (bottom-bottom contacted NW configuration), the ZnO NWs cannot undergo direct contact with the finger and therefore a polymeric encapsulating layer is required for A-III chips as well (see Fig. 18a). However, the targeted polymer layer thickness is different between the two options. In the case of A-III, a conductive layer in direct contact with the top of the NWs is implemented above the encapsulation layer in order to collect a piezoelectric signal between the top and the bottom electrodes when the NWs undergo vertical compression (Fig. 18c).

Initially, an encapsulation layer thickness slightly lower than the NWs length was targeted in order to favour direct contact between NWs top and the conductive layer. Nevertheless, it was figured out during the project that an etching step was required after the encapsulation to remove the residual dielectric polymer located at the top of the NWs and obtain an electrical signal (Fig. 18b). It was observed that the etching step removed the polymer on top of the NWs but also on other locations reducing the whole encapsulating layer thickness. Thereby, it was concluded that the targeted thickness should be higher than the NWs length and that the final encapsulation layer thickness will be mastered during the etching step (Fig. 18bc).

The main challenge here is precise controlling of polymer thickness in order to properly encapsulate NWs of pre-defined length. To do so, calibrations were performed to link spin-coating rotation speeds to polymer thicknesses. Such calibrations were performed on all types of A-III chips since it was previously demonstrated that the chip dimension, nature and contact lines organization have a significant influence on the encapsulation layer thickness. Besides, it was put into light that a primer polymer layer (low thickness, high spin-coating rotation speed) deposited below the encapsulation layer greatly improved the polymer thickness distribution on the surface. Calibration curves obtained with A-III chips (Fig. 19) show that a polymer layer thickness between 0 μm and 5 μm can be accurately controlled. It was also proven that higher thicknesses (up to 20 μm) could be obtained using a *multi-layer deposition process*.

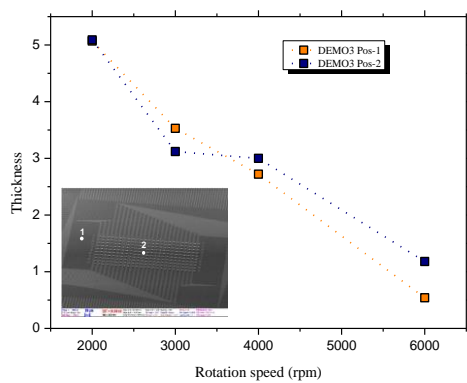


Figure 19. Polymer layer thickness as a function of the rotation speed in presence of a primer (A-III chip)

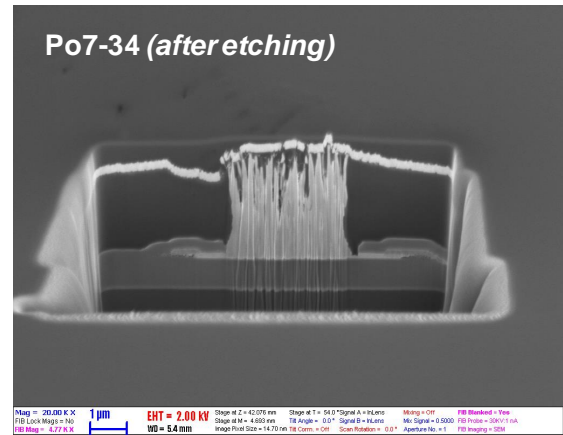


Figure 20. FIB-cut of an encapsulated A-III chip after etching and Au deposition steps with a protective polymer layer on top of the chip.

The polymer layer thicknesses were measured by ellipsometry and it was also proved during the project that such measurements were consistent with SEM measurements and micro-reflection measurements. Knowing the NWs length, it was finally possible to properly achieve the encapsulation of A-III chips. An example of SEM image obtained after encapsulation of chips with NWs of 3.5 μm is given in Fig. 20.

Fabrication of the top electrodes for A-III chips

A-III sensors require one additional fabrication step, which is the top electrode deposition on top of the insulating polymer matrix after the NW tips are liberated from the polymer using oxygen plasma etching (see Fig. 18). The metal deposition process is carried out by evaporation from the Knudsen cell at room temperature (nominal) for the polymer preservation purposes.

After the plasma processing of the polymer matrix on top of A-III chip, the active area of the chips has been covered using different conducting material. In the main route, a 100 nm thick gold layer was deposited using a conventional evaporation at room temperature. The gold shows an excellent adhesion to the polymer surface remaining flat, appropriately flexible and highly conductive in a 100 nm thickness range. The main drawbacks of this approach are related to the difference in the mechanical properties of the polymer and metal layers leading to the crack formation, especially during the mechanical probing of the sensor. This effect, however, does not affect the conductivity of the Au layer significantly, and the top electrode preserves its integrity and conducting function.

In addition, several composite conductive materials having appropriate elastic properties have been tested with A-III chips. Among them, metal nano-particles (i.e. Ag, Au & Cu) suspended in the liquid (aqua or oil) have been used as an option to the top electrode. In particular, the nano-droplet of Ag-suspension has been placed on top of the active area and dried out at the ambient conditions. The resulting layer is highly conductive consisting of Ag nano-particles weakly linked to each other. This method allows for formation of highly flexible and conductive electrode. However, the thickness of the layer is hardly controllable on the sub- μm scale.

The use of a silver based polymeric hybrid material as a top electrode is another prospective option, which has been tested, and later, conventionally used for A-III chips. The sheet resistance of silver based polymeric hybrid layers was confirmed to be very high ranging from 1 to 60 Ω/sq . The obvious advantage of this approach is identical elastic properties of the insulating and conducting polymer matrixes. The conducting polymer top

electrode was used as a stand-alone solution as well as in combination with an intermediate thin gold layer. The latter approach allows decreasing the roughness of the silver polymer surface, which is currently the main issue associated with the use of Ag nano-particles. More details on the polymer technologies and polymer material properties can be found in the following sections.

A-III-R3 sensor (alternative version): fabrication and tests

To ensure a successful demonstration of the PiezoMAT sensor technology at the end of the project, three alternative routes (R1, R2 and R3) for the finishing A-III sensors were developed and implemented. These sensors are based on the same A-III chips, but using different approaches for the fabrication of the polymer matrix and top electrode. Therefore, three groups of the A-III based demonstration sensors were fabricated and tested enumerated as *A-III-R1*, *A-III-R2* and *A-III-R3*, respectively.

In this section, the chip fabrication process for a special version of A-III-R3 (commercial photoresist and metal top contact, Fig. 21) is reported, which is based on the following technological steps: i) polymer spin-coating and hot plating, ii) etching in oxygen (or Ar) plasma until the tip of the NWs are released, iii) top metal (Au) deposition, iv) spinning of a polymer protection layer. Three conventional polymer materials were tested (SU8 negative epoxy based photoresist, PMMA e-beam resist, and S1818 positive photoresist). As a top protective layer UV exposed SU8 was used.

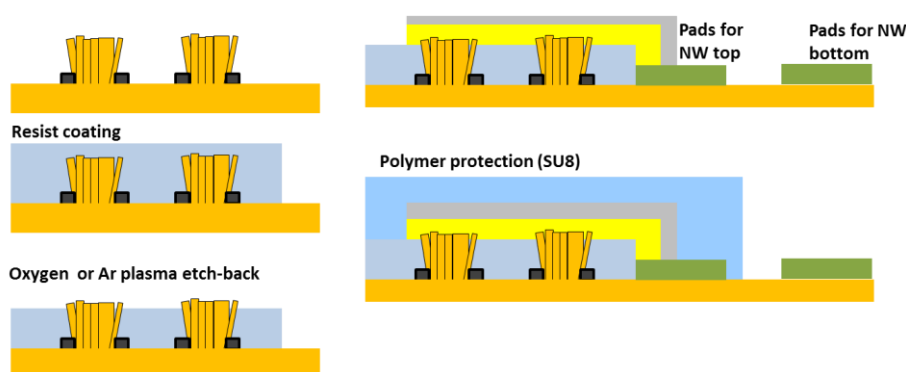


Figure 21. Schematic representation of the process steps for R3 fabrication route.

Fig. 22 shows the AFM images of a selected NW pixel before and after photoresist (S1818) encapsulation (Fig. 22a and b, respectively) and after several oxygen plasma back-etching steps (Fig. 22c). Since the tip of the NWs is free from residual polymer the chip is ready for metal deposition. Au layer of 250 nm was deposited onto the chip using e-beam evaporation method through a handmade stencil mask to obtain Schottky-type rectifying junction. (Similar results were found for PMMA, however, SU8 negative epoxy resist was found to give an unwanted residue on the top of the NWs. Though it can be removed by physical dry etching using e.g. Ar plasma due to the ion bombardment of ZnO top surface it results in an Ohmic contact with Au.) The photograph of chip in Fig. 22d shows the square shaped reddish photoresist coating and the cross-shaped yellow top metal coating which is connected to four metal pads through its arms. SEM observation of an FIB cut NW pixel confirmed the quality of the polymer encapsulation and direct contact between the top metal and ZnO NW (Fig. 22e). Before wire bonding of the chips randomly selected NW pixels were tested electrically. Most of the circuits demonstrated high quality Schottky type I-V characteristic with the expected polarity. In case of the best chip the calculated ideality factor scattered in the 2.6 - 3.6 range which is rarely found in the literature for contacted NWs.

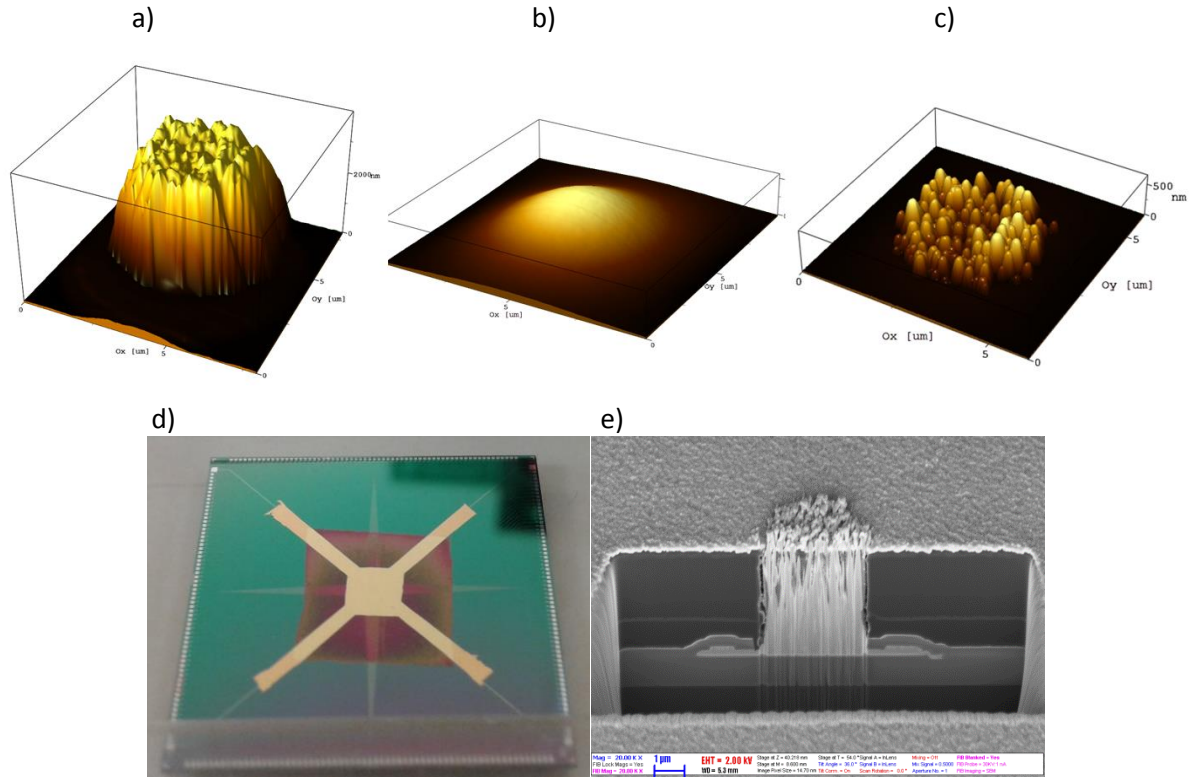


Figure 22. AFM image of a NW pixel before polymer encapsulation (a), after polymer encapsulation (b), and after etching back releasing the tip of the NWs by oxygen plasma etching (c). Photo of the fabricated chip after top Au deposition (d) and FIB cross section of a NW pixel (e).

A limited number of A-III chips (A-III-R3) were processed at MTA TTK MFA to carry out manual wedge bonding and alternative, “non-zero bias voltage” characterizations. These chips were wire bonded to a test printed circuit board with limited number of contact pads (128). Hence, roughly only every second pixel was connected among the available 250 matrix elements. In Fig. 23, macroscopic characterization setup purposely built for the alternative demonstration is shown. During the loading tests, simple stamps were pressed against active matrix of the chip ($225\ \mu\text{m} \times 600\ \mu\text{m}$). The magnitude of the loading force was continuously monitored by a calibrated force gauge (Andilog). The electrical signal of each wire bonded pixel was collected one-by-one through two ribbon cables by a high-density matrix switch which was connected to a source measure unit (National Instrument, PXI).

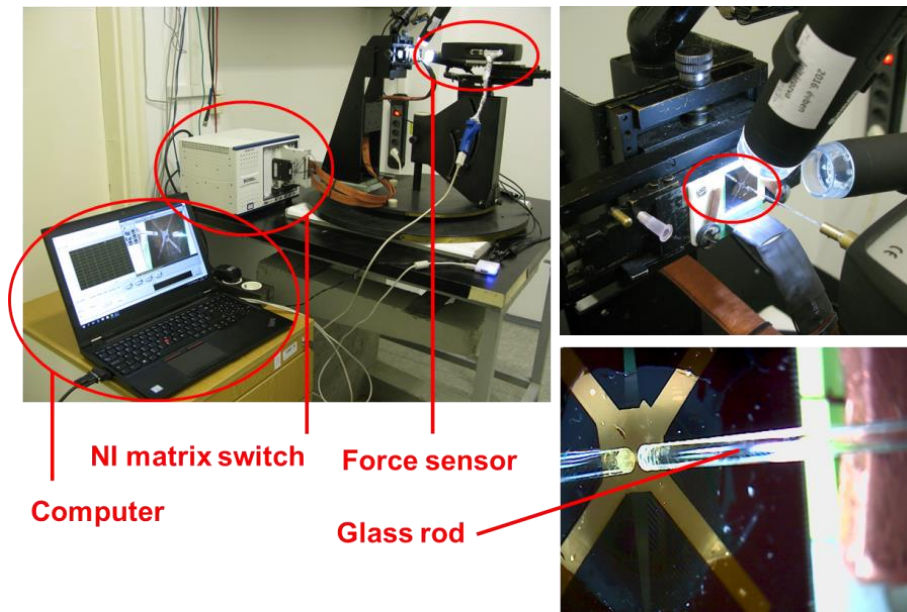


Figure 23. Macroscopic setup for pressing tests using calibrated force sensor, source measure unit connected to a 128 channel high density matrix switch (NI PXI) and a controller computer with Lab-View based data acquisition software.

A Lab-View™ based data acquisition and evaluation software was written to take I-V curves from each pixel, to monitoring time domain current/voltage signals, applying bias voltage, drawing response maps, and to monitor the signal of the force gauge. About 4.5 s is needed to collect current/voltage data for all the 128 channels at fix bias voltage/current and to refresh the chess pattern map. At first I-V curves were collected from each pixel in relaxed state. It confirmed that most of the pixels, around 117 have Schottky type rectifying curves (Fig. 24). In the selected example two pixels showed linear characteristic, while one shows a poor rectifying behaviour. By monitoring a single channel at a constant bias voltage (0.5V) under periodic loading using a glass rod type pressing stamp ($\varnothing=1$ mm) we can observe clear correlation between the applied force and the measured relative current (Fig. 25). Nevertheless, the current often shows an unwanted drift, especially in the relatively high current range ($\sim 1\text{-}10\text{ }\mu\text{A}$).

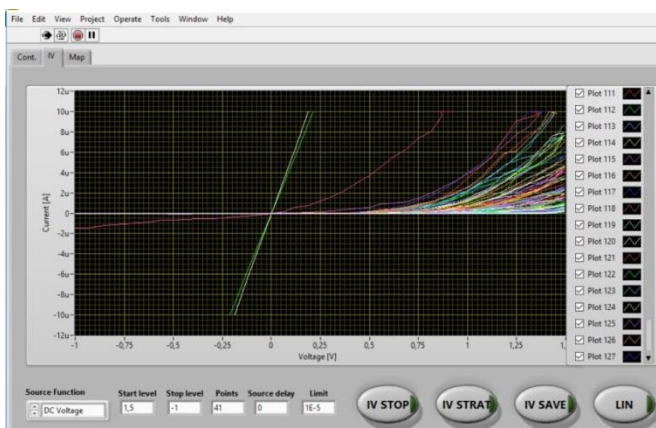


Figure 24. Snapshot taken on the controlling software showing the I-V curves of 128 pixels.

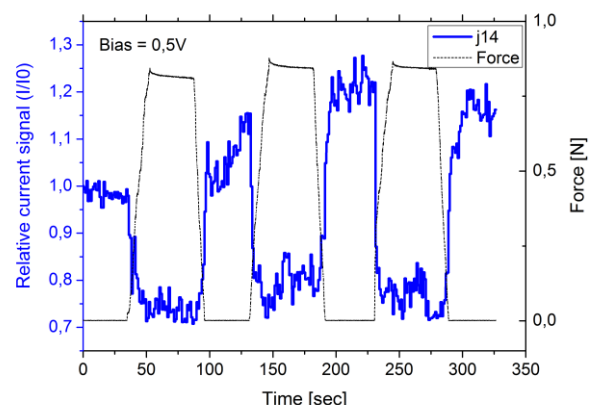


Figure 25. Time-domain relative current signal (a, blue) recorded on a randomly selected pixel (J14) with parallel monitoring of the loading force (a, black).

By applying this current monitoring method on every channel we could monitor the whole matrix and may have a chance to recognise simple patterns. However, as we found, the measurement is less noisy in current generator mode, i.e. a constant current (e.g. 100 nA) was driven through each pixel and the generated voltage was monitored and visualized by the software. Prior to pressing reference voltage (V_0) was taken from each pixel. Afterwards, only the absolute value of the relative change ($\Delta = |V_1 - V_0|/V_0$) was shown by a colour scaled matrix. In order to demonstrate pattern recognition and position sensitivity a fine Al wire was pressed ($\phi = 200 \mu\text{m}$) against the NW matrix.

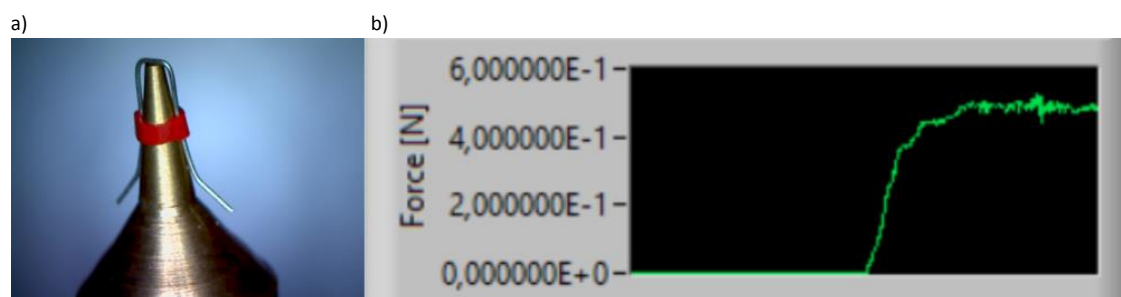


Figure 26. Pressing stamp for the pattern recognition test: fine Al wire looped around a Cu tip (a) and a typical force curve during pressing (b).

The Al wire was looped around the apex of a Cu cone mounted on the horizontal force sensor (Fig. 26a). It was aligned such a way that the long axis of the Au wire was perpendicular to the long edge ($600 \mu\text{m}$) of the rectangular matrix. During the demonstration at first the wire was pressed near to the left edge of the matrix. The applied loading force was 500 mN (Fig. 26b). After releasing the stamp it was moved manually towards the right side of the matrix along the x-axis using micro-meter positioner and pressed the matrix again. This sequence was repeated until reaching the right side of the matrix. Fig. 27 shows the colour maps taken at each loading event. Black pixels in a chess pattern indicate the un-bonded inactive elements. Deep blue colour corresponds to the unchanged voltage signal ($\Delta = 0$), while red is set to show a relative change of 7% ($\Delta = 0.07$) in this particular experiment. On the right side of Fig. 27 snapshots were taken by a USB camera to show the position of the pressing stamp relative to the chip. For clarity two dotted red lines indicate the initial and final position of the Au wire. The recorded maps on the left side clearly show the perpendicularly elongated shape of the Au wire and its position. Even though some of the unloaded pixels are also red due to the voltage drift, the pattern recognition concept, at sufficiently high loading force, seems to be feasible.

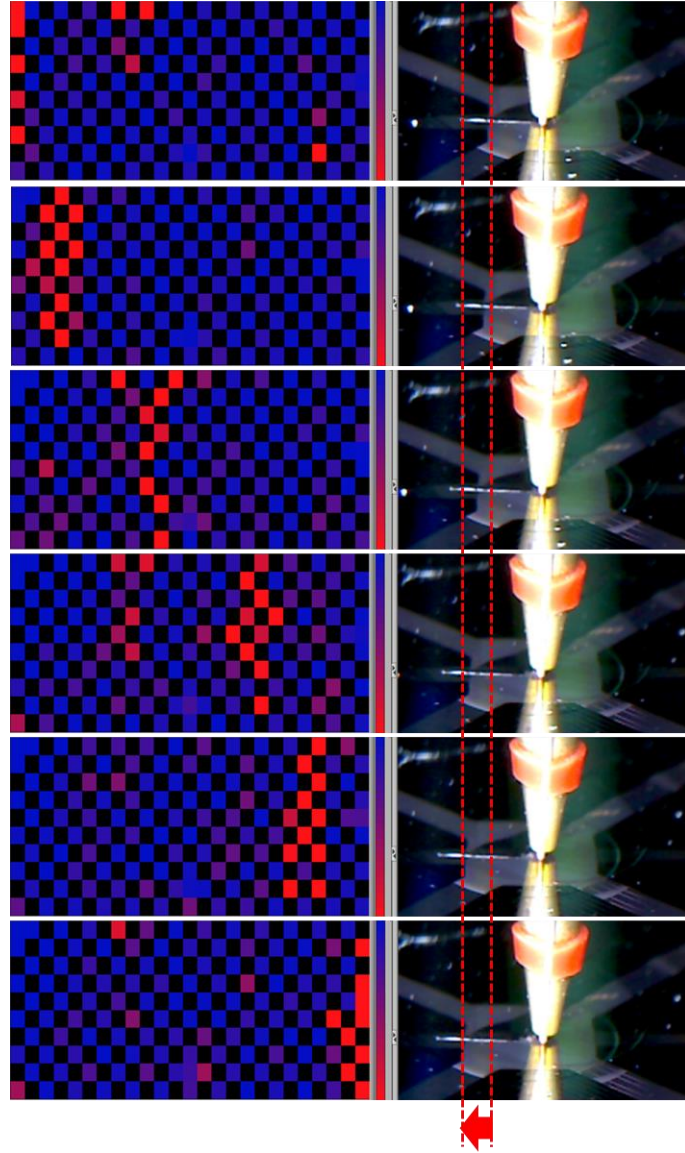


Figure 27. Relative voltage change maps at a bias current of 100 nA at different positions of the perpendicularly aligned Al wire type stamp. Position of the stamp was changed from left to right of the matrix with approximate steps of 100 μm .

A-III-R1, R2 & R3 sensors: functionality demonstration

During the sensor evaluation phase, different electrical and electro-mechanical tests were performed on 8 prepared sensor assemblies (based on A-III-R1, R2 & R3 chips) in order to characterize the electrical parameters and the sensor response. The A-III chips were connected to a Texas Instrument DDC264EVM 256-channel *Data Acquisition Board*, which was USB-interfaced with a PC to launch and collect the data. Initial characterization was done prior the sensor evaluation in order to make sure the TI DDC264 board is able to measure a signal of an expected level.

In the first series of sensing experiments, the following conditions are used: the A-III top electrode is grounded via the TI-Board ground, response measurement are performed with and without external bias, an acquisition session provides a raw data each 20 ms for total duration of 10 s. A session without contact was recorded as reference, and then, a rough rubber surface was applied several times to the chip surface with varying pressure and speed. The rubber surface is covering the entire sensing area. After these series of tests,

two specific patterns were applied to the sensor surface in order to verify a pixel response and a general pattern recognition function: grinded polycarbonate strip with a 500 μm groove and transparent polymer film with a laser printed pattern with cycles of 5 μm in diameter.

The raw data recorded by DDC256 during the pressure test with grounded A-III chips shows 5 electrical response peaks, which match the number of mechanical impacts performed during the acquisition session (Fig. 28).

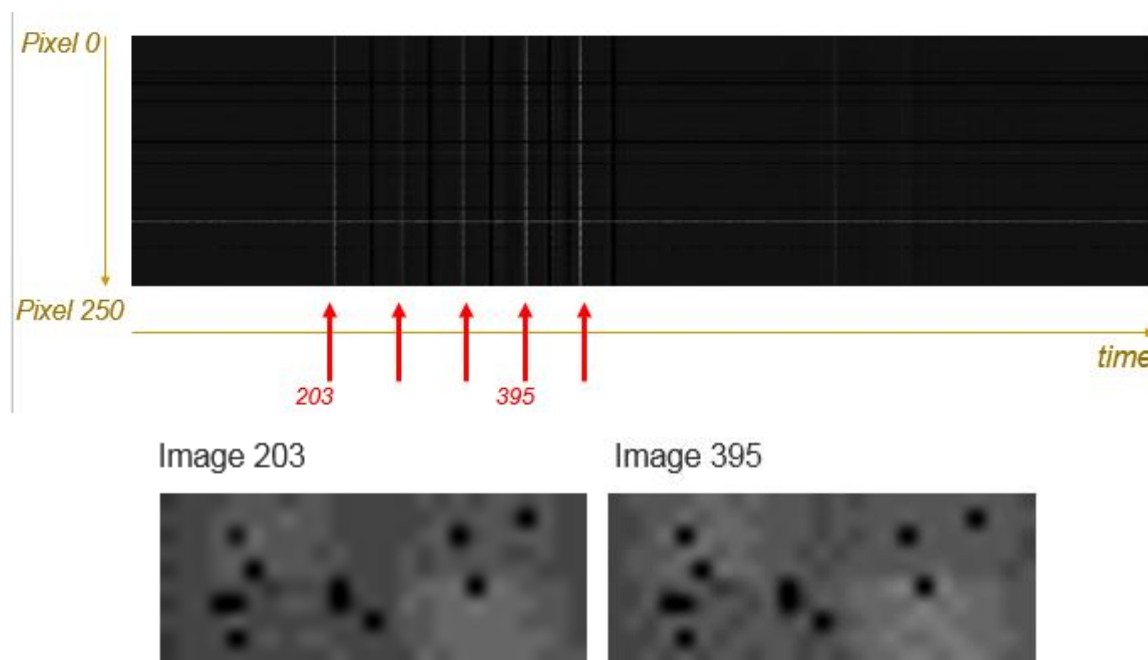


Figure 28. A-III sensor response recorded from all 256 pixels (channels) in the time domain. Images 203 and 395 are exemplary 3D maps, which were computed using A-III raw data; 25x10 matrixes were reconstructed in normalized grey-level images corresponding to the peak images 203 and 395

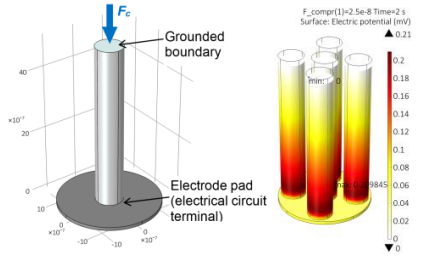
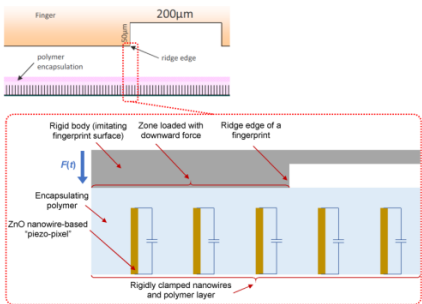
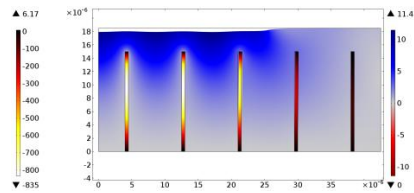
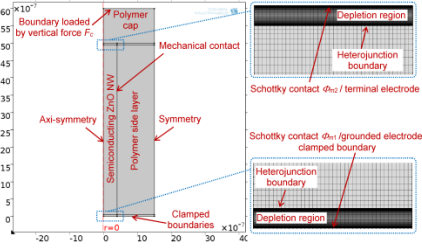
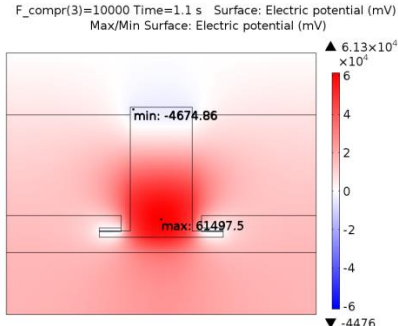
Currently:

The measured multi-channel response obtained on full-scale A-III chips (250 pixels) during application of either artificially structured surfaces or real fingerprints to the sensor do not allow recognizing 3D pattern in the images reconstructed from the raw data. These tests are currently in progress. The final results will be reported during the closing project meeting.

FEM modelling of A-III type ZnO NWs for compression force sensing (A-III)

Analogously to the case of A-II, different versions of FEM models for A-III NWs, characterized by varying degree of structural, electrical, physical and dimensional complexity, were successfully implemented (Table 2). The structural configuration of the most complex “chip-based” models (ver. FEM3.2 & FEM3.4) corresponds to the chip layout that was developed in the project and was used for the fabrication of the sensor demonstrator.

Table 2: Summary of the implemented FEM models (A-III)

Version No.	Type of model	Main features	Model images
FEM3.1	Single/multi-NW piezoelectric models (3D)	<ul style="list-style-type: none"> ▪ Idealized structural & electrical configuration (classical piezoelectric theory): <ul style="list-style-type: none"> - ZnO: dielectric. - Electrical contacts: ohmic. - Electrical properties of all dielectric and conducting stack layers accounted for. ▪ No encapsulation. 	
FEM3.2	Encapsulated multi-NW piezoelectric models (2D)	<ul style="list-style-type: none"> ▪ 2 alternatives for structural configuration: <ul style="list-style-type: none"> ▪ Idealized: no multi-layer stack, encapsulated in dielectric polymer. ▪ Realistic (chip-based): with multi-layer stack and encapsulated in dielectric & conducting polymers. ▪ 2 alternatives for mechanical coupling conditions at NW/polymer interface: rigid or contact-based (nonlinear). ▪ Idealized electrical & physical configuration: <ul style="list-style-type: none"> - ZnO: dielectric. - Electrical contacts: ohmic. - Electrical properties of all dielectric and conducting stack layers accounted for. 	 
FEM3.3	Single-NW piezo-semiconductive model (axisymmetric)	<ul style="list-style-type: none"> ▪ 2 alternatives: with/without encapsulating polymer. ▪ Idealized structural configuration: no multi-layer chip stack. ▪ Realistic electrical & physical configuration: <ul style="list-style-type: none"> - Coupled piezoelectric & semiconducting properties in ZnO. - Electrical contacts: ohmic or Schottky (nonlinear). 	
FEM3.4	Encapsulated single-NW piezo-semiconductive chip-based model (2D) /directly extendable to NW array/	<ul style="list-style-type: none"> ▪ Realistic structural configuration: NWs integrated on a multi-layer chip stack and encapsulated in dielectric & conducting polymers. ▪ Realistic electrical & physical configuration: <ul style="list-style-type: none"> - Coupled piezoelectric & semiconducting properties in ZnO. - Electrical contacts: ohmic or Schottky (nonlinear) 	

- Electrical properties of all stack layers accounted for.

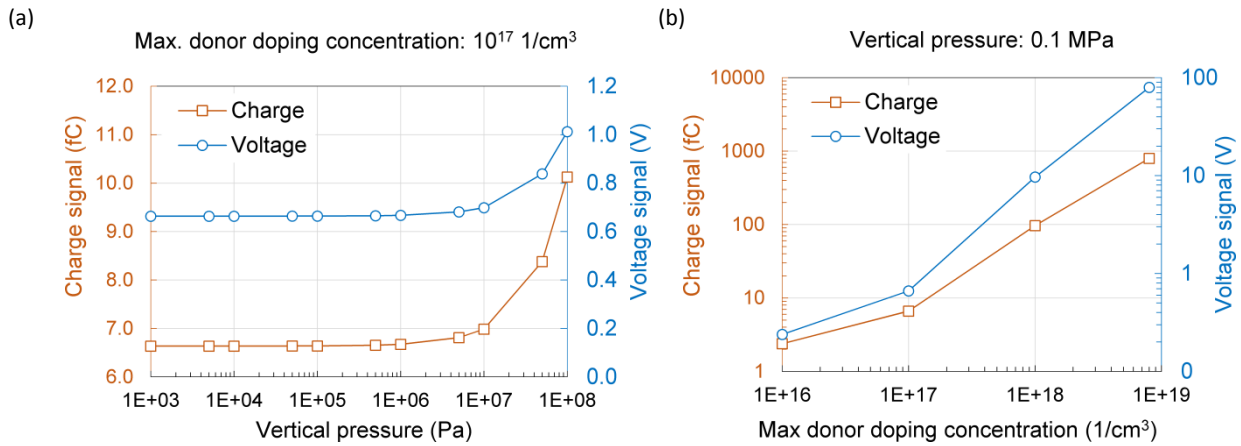


Figure 29. Representative numerical results obtained with the encapsulated single-NW piezo-semi conductive chip-based 2D model (with Schottky and Ohmic contacts at the bottom and top electrodes, respectively). The plots show variation of charge and voltage signals as a function of vertical pressure (a) and maximum donor doping concentration in ZnO (b). Model properties: NW width – $2 \mu\text{m}$, NW length – $3.5 \mu\text{m}$, external capacitor connected to NW – 10 fF .

Main results of the numerical studies for A-III NWs can be summarized as follows:

- Using the single-NW piezoelectric 3D model (ver. FEM3.1):
 - Analogously to Architecture II, the strain-induced piezoelectric charge signal from a single-NW pixel is negligible (several electrons) for the realistic pressure loads ($<50 \text{ kPa}$).
 - The piezoelectric signal “per pixel” may be successfully magnified by using an NW array.
 - Increase of the horizontal force component has insignificant effect on the piezoelectric signal (this is valid only for the un-encapsulated NW).
- Using the encapsulated multi-NW piezoelectric 2D models (ver. FEM3.2):
 - Near-optimal values of the encapsulating polymer Young’s modulus were predicted to be in the range of about $0.2 - 0.5 \text{ GPa}$ (irrespective of NW aspect ratio and pressure load orientation). The recommended near-optimal values of polymer cap height are in the range of about $2 - 4 \mu\text{m}$ (irrespective of NW aspect ratio for the predominantly compressive loads). At these near-optimal values, the useful piezoelectric signals are maximized and the parasitic (spurious) signals – minimized.
 - Compared to Architecture II, NW array of Architecture III exhibits less complex and more favourable electromechanical behaviour when subjected to varying input parameters (e.g. NW aspect ratios, load orientations). For example, spurious signals in this case are considerably lower, which implies higher native spatial resolution in comparison to the analogous implementation of Architecture 2 fingerprint sensor.
- Using the single-NW piezo-semiconductive axisymmetric model (ver. FEM3.3):
 - Due to incorporation of the semiconductor physics effects, the generated strain-induced piezoelectric charge signal is tens of times lower in comparison to the signal predicted by the classical piezoelectric model (ver. FEM3.1).
 - Force-dependent electrical signals from a single NW are observed only when tensile strain exceeds about 0.1% , which is consistent with strain levels for which the experimental results on single NWs are reported in the literature.⁷

⁷ S. Xu, Y. Qin, C. Xu, et al. Self-powered nanowire devices. *Nature Nanotechnology*, vol. 5(5), p. 366-373, 2010.

- It is important to maximize the strain rate in order to increase the current signal to the level that is exploitable by the readout electronics.
- Using the encapsulated single-NW piezo-semiconductive chip-based 2D model (ver. FEM3.4) with Schottky and ohmic contacts at the bottom and top electrodes, respectively (ZnO NW pixel size is $3.5\ \mu\text{m} \times 2\ \mu\text{m}$):
 - The predicted trends of variation of electrical signals with the increasing pressure load (Fig. 30) implies that two operation modes could be distinguished with respect to the magnitude of applied load (for pixel diameters of several micrometers!):
 - a) In low-load range (roughly: $<1\ \text{MPa}$) the sensor operates in *force-activated regime*, which essentially corresponds to the binary sensing mode. In this load range the electrical signals have relatively high magnitude that cannot be attributed to the strain-induced piezoelectric effect and are insensitive to the increasing compression load. Force-dependent signals in the low-load range could be potentially attained by: i) (significantly) increasing pixel area to obtain parallel-connection of the NWs, thereby enabling increase of the charge and current outputs), ii) series-connecting the pixels, thereby enabling increase of the voltage output.
 - b) In high-load range (roughly: $>1\text{--}2\ \text{MPa}$) the sensor operates in *force-dependent regime* since the electrical signals become sensitive to the increasing load (force-dependency is considerably stronger in comparison to the Architecture 2 model ver. FEM2.3). Analogously to the low-load case, the predicted relatively high electrical outputs cannot be attributed to the piezoelectric effect alone. Due to very high loads required, this regime is not suitable for fingerprint sensing, but could be potentially applied in high-resolution tactile sensing in industrial applications (e.g. in robotic skin).
 - c) The predicted relatively high electrical signals generated by the modeled Schottky-contacted piezo-semiconductor/metal sandwich microstructure suggest that the strain-induced piezo-charges might not be the primary factor contributing to the mechanical-to-electrical energy conversion process. State of the art review reveals that the fundamental underlying mechanism of this process is not yet fully understood in terms of the piezotronic effect [ref. 3]. Some of the best candidate explanations include strain-dependent modification of potential barrier height of the Schottky contact, increased electron density and reduced resistance in ZnO under compression.^{8,9}
 - The predicted sensitivities are as follows: voltage – $3.5\ \mu\text{V/kPa}$, charge – $3.5 \times 10^{-5}\ \text{fC/kPa}$, current – $7.8 \times 10^{-4}\ \text{fA/kPa}$. Voltage sensitivity is comparable to the experimental values reported in the literature for the hydrothermally-grown ZnO NW arrays: $\sim 1\text{--}5\ \mu\text{V/kPa}$ for the tactile pressure sensor (pixel size: $500\ \mu\text{m} \times 500\ \mu\text{m}$)¹⁰ and $\sim 8\ \mu\text{V/kPa}$ for the large-area nanogenerator (pixel size: $\sim 4\ \text{mm}^2$) (see Xu et al.).
 - Magnitude of electrical signals strongly depends on the maximum donor doping (n-type) concentration in ZnO (Figure 3.4.12): the most pronounced increase is predicted for $10^{18}\text{--}10^{19}\ \text{1/cm}^3$. The predicted charge signal at $10^{18}\ \text{1/cm}^3$ is on the order of 100 fC, which is in agreement with the signal levels measured on the demonstrator.

⁸ P. Keil, T. Froemling, A. Klein, et al. Piezotronic effect at Schottky barrier of a metal-ZnO single crystal interface. Journal of Applied Physics, vol. 121(15), 155701, 2017.

⁹ R. Baraki, N. Novak, M. Hofstaetter, et al. Varistor piezotronics: Mechanically tuned conductivity in varistors. Journal of Applied Physics, vol. 118(8), 085703, 2015.

¹⁰ B.P. Nabar, Z. Celik-Butler, D.P. Butler. Self-Powered Tactile Pressure Sensors Using Ordered Crystalline ZnO Nanorods on Flexible Substrates Toward Robotic Skin and Garments. IEEE Sensors Journal, vol. 15(1), p. 63-70, 2014.

3.5 Conclusion

An expected paradigm shift in the fingerprint sensor technology for the last five years is a necessity to obtain a *3D topology* of the finger surface with a *very high lateral resolution*: emerging sensors should resolve *in situ* the smallest 3D topographies with a characteristic dimension of several micro-meters. Reported PiezoMAT sensor combines these two distinctive features in one integrated device – real-time high-resolution pressure sensing from 3D surfaces. During the 44 month of the project duration, PiezoMAT has been unifying the efforts of 8 consortium partners from European research and industry to achieve an ambitious technical goal announced in 2013 – realization of absolutely novel sensing concept and implementation of fabrication technology for a new generation of high-resolution fingerprint sensors for emerging portable devices. Coordinated by CEA Leti, the EU PiezoMAT consortium includes two universities (Leipzig, Kaunas), three research institutions (Tyndall, Fraunhofer, Institute of Technical Physics and Materials Science) and two industrial partners (Specific Polymers and Morpho). The compact consortium with a highly complementary character was built to provide extensive research in four main technical development areas, which are essential for achieving final project's goal:

CEA Leti – *administrative coordination along with electronic design and wafer-scale processing;*

Fraunhofer IAF – *technical coordination and micro-electro-mechanical characterisation of the sensors;*

MTA TTK MFA – *NW growth, wafer-scale processing along with characterization of the sensors;*

Morpho – *end-user company responsible for all technical specification and sensor prototyping;*

Specific Polymer – *development of unique polymer coating perfectly matched to the sensing function;*

Tyndall Institute – *unique nano- deposition & characterization technologies powered by development of analytical models for ZnO NW based sensors;*

Kaunas University – *multi-parameter behavioural numerical models taking into account piezo-semiconducting and mechanical properties of ZnO NWs embedded into the polymer matrix.*

University of Leipzig – *material characterization, ZnO growth and its integration into conventional silicon wafer processing;*

The PiezoMAT fingerprint sensor is a “direct-touch” device based on array of ZnO NWs combined into an addressable 2D matrix. Here, a 2D resolution is conservatively determined by the density of pixel-array elements. It is defined merely by the distance between adjacent ZnO-NW-pixels, which are fabricated on the patterned 200 mm Si wafers. The main technical challenge at this stage - ***the solid integration of ZnO NW pixels into a conventionally processed silicon chip*** – was successfully solved by CEA in close cooperation with the University of Leipzig and MTA TTK MFA in the field of wafer scale ZnO deposition and ZnO NW growth, respectively. The lateral (2D) resolutions of 5000 dpi and 1000 dpi achieved on A-II and A-III sensors, respectively, exceed greatly the resolution of the current “main-stream” fingerprint devices.

As mentioned above, the distinctive feature of the PiezoMAT sensor is related to the unique construction of the ZnO NW pixels. ZnO NWs are piezo-semiconductor nano-devices capable to change electrical characteristics upon bending or compression of the NW by applying a mechanical load. The level of generated electrical signal is dependent on the locally applied force, and therefore the 3D profile of the fingerprint can be mapped simultaneously by acquiring the electrical signal magnitude from each pixel. The solution for the major technical challenge - ***highly controllable growth of ZnO NW precisely at the lithographically defined nucleation sites*** - was developed by MTA TTK MFA. In close cooperation with other partners they proved that *wet chemical selective growth* is reliable and highly-productive technique for the fabrication of ZnO NWs on micro-patterned silicon substrates.

As the ZnO NWs, due to their nano-dimension, are highly fragile objects and cannot sustain a direct mechanical load from the finger, a safe protection of the array with an elastic layer (*the encapsulation*) is an essential step to maintain sensor long-term functionality. The complex development of ***polymer layers with predefined elastic properties*** along with technologies for the precise coating of the sensors was a challenging task for

Specific Polymers. The polymer matrices with an improved elasticity and high chemical inertness were designed and tested on two consequent generations of the PiezoMAT sensors (A-II and A-III). In addition, the silver-doped conductive polymer designed by Specific Polymers was employed as a flexible top electrode for the last generation sensors.

From the beginning of the research, the consortium was strongly focused on developing highly reliable sensor devices, which can be rapidly marketed as well as on fabrication technologies, which are directly relevant for the industrial production of the sensors. Therefore, PiezoMAT program was built exploring different sensor designs with a gradually increasing level of technological challenges. Three different sensor architectures were designed and studied. In particular, *Architecture I* represents a fundamental research level employing electron-microscopy-based nanotechnologies for electrode fabrication and electrical characterisation. These studies are carried on stand-alone ZnO NWs in the Tyndall Institute. The A-I development lead to the significant progress in the application of *electron beam induced deposition* for the nano-electrode fabrication and *in situ* characterisation of the nano-devices. The data obtained on A-I sensors was used promptly in the sensor modelling tasks. In addition, several research papers were published by the consortium partners based on the findings originating from A-I research.

Most technologically complex, “bottom-bottom” contacted A-II devices are micro-fabricated in MTA TTK MFA. These sensors are initially designed for the ultra-high-resolution fingerprint sensing (> 5000 dpi). Despite being extremely complex in electrode configuration and very demanding to the fabrication accuracy, A-II sensor arrays demonstrate reproducible detection performance. Its constructive particularities (i.e. no top-contact leading to free NW tips), allow for the use of A-II in different sensing applications. Here, the change of electric properties of ZnO NW upon electro-chemical impact can be exploited in photo-, gas- and bio-sensing. As the NW growth method is not limited only by ZnO, A-II is a quite flexible solution for the various sensor devices, where real time acquisition of 2D data from the limited area is essential for the analyses, i.e. “electronic nose” and “artificial skin” applications.

The micro-fabrication and tests of PiezoMAT devices were extensively powered by theoretical modelling of the sensors using analytical and numerical approaches developed by Tyndall Institute and Kaunas University, respectively. ZnO properties at nano-scale as well as NW electro-mechanical behaviour are subjects of the intensive discussions in the scientific community, often based on fully controversial experimental results. Therefore own models taking into account “unconventional” modelling parameters, i.e. elastic properties of the polymer matrix, spontaneous polarization phenomena and “piezo-semiconducting” properties of ZnO NWs, were appeared to be extremely useful and powerful tools for the evaluation and design purposes.

Based on the A-I and A-II development, diverse versions of A-III based sensors were finally fabricated by the consortium and tested towards pattern recognition functionality. Due to their higher reliability and lower fabrication complexity (as compared to the A-I & II types), A-III sensors were chosen for the final validation of the sensor functionality in a “quasi-operational” environment. Till now, a 3D pattern recognition function was validated on a simplified sensor configuration acquiring the data from 128-channel. The full-scale 250-channel sensor assemblies are currently under test. The final results are intended to be reported during the closing project meeting.

4. Potential impact, main dissemination activities, exploitation of results

Scientific and technical impact to the research market

During the PiezoMAT project, a number of intriguing scientific findings and technical know-hows have been recognised, classified and finally disseminated. The achieved results and *know-how's* come from different knowledge fields ranging from wafer-scale integration technology to polymer synthesis and numerical sensor models. Moreover, from the beginning of the project, the consortium was strongly focused on developing highly reliable sensor technologies and architectures, which are directly relevant for the industrial-scale production. Therefore, a potential impact also originates from multiple development areas, e.g. related to the final sensor device or intermediate products obtained during R&D.

Due to ambitious goals and high technological complexity of the device, the consortium faced numerous technological and methodological challenges, which have been identified and solved by the PiezoMAT team. The developed by consortium partners technical solutions are valuable know-hows. It is important to note that these findings and tools have mostly universal character and can be employed in various emerging electronic and non-electronic devices, being not limited by only to the fingerprint sensor applications based on ZnO NWs. In the following Table, the main *technological* and *scientific* achievements of the PiezoMAT consortium are listed together with their expected (potential) impact to the research (and consumer) market:

#	Result	Potential Impact
1	“Direct-touch” fingerprint sensor architecture with a spatial resolution of > 5000 dpi (A-II)	PiezoMAT proposes a new, scalable technology for fingerprint sensors, ensuring sufficient resolution to detect level 3 fingerprint features such as pores and ridge edges. Such level of resolution considerably strengthens the reliability of fingerprint reading and enables security reinforcement regarding biometric identification. However, in the current version, a small area sensor is realized as a stand-alone device with non-integrated electronic acquisition part. For the real applications, the sensor active area should be significantly enlarged, and therefore, requires integrated electronic circuits for the acquisition, amplification and processing of the electronic response.
1	Technology for manufacturing addressable, ultra-high-resolution matrices based on compound semiconductor pixels solidly integrated into Si circuits	The developed technologies are designed, but not limited to the ZnO NWs so as a variety of materials can be deposited by wet chemical growth method. Therefore, directly addressable, ultra-high-resolution sensor platform can be adjusted for wide range of the emerging sensors requiring spatial information with micrometer accuracy, e.g. bio-metric sensors, neurological bio-sensors along with “electronic skin” and “electronic nose” applications.
2	Wafer-scale add-on technology for solid integration of ZnO functional components into a conventionally processed silicon chips	In PiezoMAT, high productivity methods for a wafer-scale deposition of high quality, single-crystalline ZnO seed layers and nano-wires on patterned Si substrates were developed. A wide spectrum of the devices requiring “compound semiconductor” micro-components to be solidly integrated “on-Si-chip” might benefit from the developed technology. Especially, it is suited for

the integration of piezo-electric micro-devices in high-tech applications, e.g. ZnO (or AlN) electro-acoustic filters for RF electronics and ultrasonic emitters and detectors for Piezoelectric Micro-machined Ultrasonic Transducers (PMUT). In addition, owing to compatibility with 8" Si-wafer micro-machining, this technology can be easily adapted for the fabrication of already established MEMS devices to increase the integration density and to add extra functionality of e.g. accelerometers, motion sensors, micro-mirror arrays, etc.

- | | | |
|---|---|---|
| 4 | Production of insulating polymer coating with predefined elastic, chemical and optical properties matched to the specific "operational environment" requirements; | Matching mechanical, chemical and optical properties of polymer coating to the specific application needs can be an effective tool in numerous fields ranging from food production monitoring and environmental sensors to the functional coating in car- and aero-space industries. An actual example is a protection coating for the sensors in the aggressive environments with a limited friction, e.g. electronic pH- or process-monitoring sensors in food and pharma industry. |
| 5 | Fabrication method for high-conductivity silver-doped polymer coating, | Non-toxic in production and chemically inert flexible top electrode for large-area (i.e. wearable) energy harvesting and sensor applications; |

Theoretical modelling using analytical and numerical approaches is most valuable contribution to the physics knowledge database from the PiezoMAT project. ZnO properties at nano-scale as well as NW electro-mechanical behaviour are subjects of the intensive discussions in the scientific community, often based on fully controversial experimental results. High quality ZnO NW samples and the experimental results obtained on these structures were used as a solid basis for building of comprehensive behavioural models taking into account "unconventional" modelling parameters, i.e. elastic properties of the polymer matrix, spontaneous polarization phenomena and "piezo-semiconducting" properties of ZnO NWs. These models appeared to be extremely useful and powerful tools for the evaluation, design and dissemination purposes.

To complete the consideration of S/T impact from the PiezoMAT project to the research market, it is also important to highlight specific roles of each consortium partner in the creation of the engineering and scientific know-hows obtained in the course of this research:

- KTU and Tyndall: development of series of novel numerical and analytical models accounting for the piezo-semiconducting properties of encapsulated electro-mechanical arrays based on ZnO NWs;
- CEA, ULEI & MTA TTK MFA: development of unique wafer-scale add-on technologies for the ZnO integration into a conventional CMOS processing;
- MTA TTK MFA: development of high-speed selective growth of high-quality ZnO NWs on patterned CMOS substrates;
- ULEI: the growth of ultra-thin ZnO nano-wires;
- SP: development of polymers with predefined mechanical, chemical and electrical properties along with polymer deposition processes on nano-structured surfaces;
- Fraunhofer: implementation of new electro-mechanical probing methods for ultra-precise electrical analyses of piezo-semiconductor nano-devices;
- Morpho: development of technical requirements to the new generation fingerprint sensors; design of electronic circuitry for acquisition of the ultra-low (fC) electrical signals in sensor operational environment

& construction of data acquisition module; development of new methodology and software for ultra-high-resolution fingerprint analyses.

Socio-economic impact and the wider societal implications of the project

Fingerprint sensors, and more generally biometric technologies, have taken since a few years a growing place in society in various domains and applications: government solutions (police, border control, and identity issuance), access control, and more recently business solutions (banking and e-commerce), health, mobile phones, etc. The PiezoMAT project is exploring a completely new technology to develop fingerprint scanners. Their advantages are very high resolution and a very small sensor size. The need for higher resolution and small volume occupation sensors that drives the project was clearly formulated by actors of the fingerprint sensor industry, especially with the growing market of fingerprint scanners for mobile phones. The opportunity for new technologies in the fingerprint sensor domain is real if we consider the large panel of competing technologies on the market or emerging.

However, when it comes to social-economic domain, it raises the more general question of the impact on society of the increasing use of biometric technologies, with fingerprint recognition in the first place. While biometrics emerged since several years from now and is more and more implemented along with legal frameworks, this particular question of societal impact is still heavily discussed nowadays. The increasing use of biometric systems has broad social ramifications and one overarching consideration is proportionality. While the technical and engineering aspects of a system that contribute to its effectiveness are important, it is also useful to examine whether a proposed solution is proportional and appropriate to the problem it is aimed at solving. Biometric systems' close connection to an individual, as described in the preceding section, means that even extremely effective technical solutions may turn out to be inappropriate due to perceived or actual side effects and means that proportionality—both how the system will be perceived in its user communities as well as possible side effects, even if the system is accurate and robust—must be considered when first examining the solution space.

Where biometric systems are used extensively, some members of the community may be deprived of their rights. Some individuals may not be able to enrol in a system or be recognized by it as a consequence of physical constraints, and still others may have characteristics that are not distinctive enough for the system to recognize. There will also be those who decline to participate on the basis of religious values, cultural norms, or even an aversion to the process. Religious beliefs about the body and sectarian jurisdiction over personal characteristics (e.g. beards and headscarves) or interpersonal contact (e.g. taking photographs, touching or exposing parts of the body) may make a biometric system an unacceptable intrusion. Mandatory or strongly encouraged use of such a system may undermine religious authority and create de facto discrimination against certain groups whose members are not allowed to travel freely, take certain jobs, or obtain certain services without violating their religious beliefs. Another category of people who may choose not to participate are those concerned about misuse or compromise of the system or its data—and its implications for privacy and personal liberty. Although a decision to participate or not may be an individual one, biometric systems can inadvertently affect groups whose shared characteristics make them less inclined to use the systems, assuming that participation is voluntary. Where use is mandatory, even more consideration of these issues may be needed.

A community, including those not affected directly, may come to distrust the systems or the motivations of those deploying them. A system deployed in a community in which certain members are consistently unable to participate in the de facto methods of recognition without significant inconvenience may acquire an unwelcoming reputation no matter how benign the purposes for which it is deployed.

Biometrics also raises some privacy concerns. Biometric systems have the potential to collect and aggregate large amounts of information about individuals. Almost no popular discussion of biometric technologies and systems takes place without reference to privacy concerns, surveillance potential, and concerns about large databases of personal information being put to unknown uses. Privacy issues arise in a cultural context and have implications for individuals and society even apart from those that arise in legal and regulatory contexts. The problems arising from aggregating information records about individuals in various information systems and the potential for linking those records through a common identifier go well beyond biometrics, and the challenges raised have been addressed extensively elsewhere.

Nonetheless, to cope with those issues regarding social acceptance, important initiatives and work have been conducted by European Union, the member states and the biometric companies to enhance the perception of biometric technologies by the public, especially through the establishment of working group addressing privacy issues and the adoption of specific policies regarding personal data protection. In more in details we can mention the following aspects:

Regulation: The past 25 years have seen several waves of data privacy regulation around the world, with mature markets revising their legal regimes and emerging markets passing new laws. All these laws regulate, to a greater or lesser extent, how organizations and governments handle personal data and are all based on common principles such as:

- transparency and control—the individual must be told about the use of their personal data and they must be able to control that use;
- purpose limitation—the personal data can only be used for the original purpose;
- security—the personal data must be protected against unauthorized or accidental disclosure;
- data quality—the personal data collected must be appropriate for the task in hand, accurate and kept up to date.

Practice: Practice has changed. Governments and organizations are much more aware than they used to be, not only of the danger of ignoring data privacy requirements, but also of the reputational and commercial benefits of handling personal data wisely.

Familiarity: Individuals have had to familiarize themselves with an ever-changing world: global outsourcing of business processes, the Internet and social media have all been embraced and absorbed by a responsive public. Indeed, biometrics is “just another frontier” in the changing technology landscape.

Additionally, if the adoption of biometrics is now experiencing such growth, it’s because it can offer various benefits, including:

Enhanced security: the IEEE among others, refers to biometrics as the “strongest” of the three authentication steps mentioned previously, due to:

- Strength and non-repudiation: Users select passwords that they easily remember, and/or write down. Tokens can often be duplicated, borrowed or stolen. Unlike a password, it is rare that the user will have the option of choosing a “bad” (insecure) biometric feature to enrol. Biometric features are unique, meaning biometric authentication offers limited deniability.
- Usage motivation: Often users are the weakest link in a security process—they may not be interested, nor see the need for, some security measures. Biometrics can increase adherence to security policies by being less inconvenient and offering a positive user experience. This improved experience can motivate users to take full advantage of the security mechanisms, instead of attempting to circumvent them.

Increased convenience: in general, citizens are not interested in security— rather, they want to go about their business with minimal inconvenience. Biometrics can help them achieve this, by enabling faster, more streamlined, and more natural user interaction with a system, mimicking how people recognize and trust people they know. Furthermore, users are not able to forget their biometrics, or leave them at home.

- Reduced cost: incorporating biometric recognition into a system comes with a certain investment cost; when deployed correctly, it will offer opportunities to reduce operational costs, through simplified processes, self-service automation (giving a decreased need for manual work), and reduced maintenance (such as removal of the need to maintain or replace smartcard tokens and readers).
- Greater inclusion: in many developing countries, people live without official identities, or the ability to prove them. Access to many services relies upon the provider being able to identify a person— without an “official” identity it is hard to open a bank account, apply for a loan, or prove eligibility to government benefits. Effective identification of citizens brings benefits for governments, allowing them to maintain service delivery, help optimize service provision, and reduce fraud, in areas such as healthcare, food subsidies, border control, or taxation. In short, inclusion-related benefits derived from biometric systems can accrue to both governments and their citizens.

Coming back to PiezoMAT sensor prototype, it is still too early given the current maturity of the technology to precisely know the potential socio-economic impact. The important growth of the biometric market during the last 15 years had itself an important societal and economic impact as discussed above. From the economic perspective, the PiezoMAT technology can probably, once at an industrial level, attract a significant share of the fingerprint sensor market, especially for mobile devices. As a fingerprint sensor, PiezoMAT technology is not expected in itself to be a strong driver for societal changes, but it will participate to the wider trend of biometrics in changing society habits as well as providing solutions for more security and convenience.

- END OF REPORT -

5. Use and dissemination of foreground

NO.	Title	Main author	Title of the periodical or the series	No	Publisher	Year of publication	Relevant pages	Permanent identifiers ¹¹ (if available)	Is/Will open access ¹² provided to this publication?
1	Low-Temperature PLD-Growth of Ultrathin ZnO Nanowires by Using $Zn_xAl_{1-x}O$ and $Zn_xGa_{1-x}O$ Seed Layers	Alexander Shkurmanov	Nanoscale Research Letters	12	Springer	2017	134-141	https://nanoscalereslett.springeropen.com/articles/10.1186/s11671-017-1906-2 doi : 10.1186/s11671-017-1906-2	yes
2	Selective growth of tilted ZnO nanoneedles and nanowires by PLD on patterned sapphire substrates	Alexander Shkurmanov	AIP ADVANCES	6	AIP Publishing	2016	095013-1 - 095013-5	http://aip.scitation.org/doi/10.1063/1.4963076 doi: 10.1063/1.4963076	yes
3	Contacting ZnO Individual Crystal Facets by Direct Write Lithography	Nikolay Petkov	ACS Appl. Mater. Interfaces	8	American Chemical Society	2016	23891–23898	http://pubs.acs.org/doi/abs/10.1021/acsami.6b05687 doi: 10.1021/acsami.6b05687	no
4	Static Finite Element Modeling for Sensor Design and Processing of an Individually Contacted Laterally Bent Piezoelectric Nanowire	Edgar A. A. Leon Perez	IEEE T. on Nanotechnol.	15 (3)	IEEE	2016	521-526	http://ieeexplore.ieee.org/document/7445219/ doi:: 10.1109/TNANO.2016.2549064	no
5	Nondestructive atomic compositional analysis of BeMgZnOquaternary alloys using ion beam analytical techniques	Zsolt Zolnai	Applied Surface Science	327	Elsevier	2015	43–50	http://www.sciencedirect.com/science/article/pii/S0169433214025409 doi: 10.1016/j.apsusc.2014.11.067	no

¹¹ A permanent identifier should be a persistent link to the published version full text if open access or abstract if article is pay per view) or to the final manuscript accepted for publication (link to article in repository).

¹² Open Access is defined as free of charge access for anyone via Internet. Please answer "yes" if the open access to the publication is already established and also if the embargo period for open access is not yet over but you intend to establish open access afterwards.

TEMPLATE A2: LIST OF DISSEMINATION ACTIVITIES								
NO.	Type of activities ¹³	Main leader	Title	Date/Period	Place	Type of audience ¹⁴	Size of audience	Countries addressed
1	Manuscript - submitted to ACS Appl. Mater. Interfaces	A.Bouvet-Marchand	Design of UV-Crosslinked Polymeric Thin Layers for Encapsulation of Piezoelectric ZnO Nanowires for Pressure-Based Fingerprint Sensors	-	-	-	-	World
2	Manuscript - submitted to Nano Energy	Masoud Seifikar	Direct observation of spontaneous polarization charge transfer in stressed ZnO nanorods	-	-	-	-	World
3	Manuscript - under preparation	J. Radó	Integrated piezoelectric nanowire arrays for high resolution tactile mapping	-	-	-	-	World
4	Conference and publication - Eurosensors XXX (oral)	Elise Saoutieff	Integration of piezoelectric nanowires matrix onto a microelectronics chip (Proc. Eng, 168, 1638-1641, 2016) doi: 10.1016/j.proeng.2016.11.479	Sept. 2016	Budapest, Hungary	Scientific Community		EU
5	Conference and publication - Eurosensors XXX (poster)	Björn Christian	Piezo-force and vibration analysis of ZnO nanowire arrays for sensor application (Proc. Eng, 168, 1192-1195, 2016) doi: 10.1016/j.proeng.2016.11.406)	Sept. 2016	Budapest, Hungary	Scientific Community		EU
6	Conference and publication - Eurosensors XXX, (poster)	A.Bouvet-Marchand	UV-crosslinked polymeric materials for encapsulation of ZnO nanowires in piezoelectric fingerprint sensors (Proc. Eng, 168, 1136-1139, 2016) doi: 10.1016/j.proeng.2016.11.374)	Sept. 2016	Budapest, Hungary	Scientific Community		EU
7	Conference and publication - Eurosensors XXX, (poster)	Alexander Shkurmanov	Growth kinetics of ultrathin ZnO Nanowires grown by Pulsed Laser Deposition (Proc. Eng, 168, 1156-1159, 2016)	Sept. 2016	Budapest, Hungary	Scientific Community		EU

¹³ A drop down list allows choosing the dissemination activity: publications, conferences, workshops, web, press releases, flyers, articles published in the popular press, videos, media briefings, presentations, exhibitions, thesis, interviews, films, TV clips, posters, Other.

¹⁴ A drop down list allows choosing the type of public: Scientific Community (higher education, Research), Industry, Civil Society, Policy makers, Medias, Other ('multiple choices' is possible).

			doi: 10.1016/j.proeng.2016.11.387					
8	Conference and publication - Eurosensors XXX, (poster)	Rolanas Dauksevicius	Finite element analysis of polymer- encapsulated ZnO nanowire-based sensor array intended for pressure sensing in biometric applications (Proc. Eng, 168, 864- 867, 2016) doi: 10.1016/j.proeng.2016.11.292	Sept. 2016	Budapest, Hungary	Scientific Community		EU
9	Conference and publication - EuroSimE	Rolanas Dauksevicius	Numerical study of near-optimal parameters of polymeric encapsulation layer containing a periodic array of piezoelectric nanowires used for force sensing (IEEE) doi: 10.1109/EuroSimE.2016.7463342	18-20 April 2016	Montpellier, France	Scientific Community		EU
10	Conference and publication - Eurosensors XXIX)	Rolanas Dauksevicius	Multiphysics model of encapsulated piezoelectric-semiconducting nanowire with Schottky contacts and external capacitive circuit (Proc. Eng, 120, 896-901, 2015) doi: 10.1016/j.proeng.2015.08.777	6-9 Sept. 2015	Freiburg, Germany	Scientific Community		EU
11	Conference and publication - 15th IEEE-Nano (oral)	Masoud Seifikar	Enhanced pressure response in ZnO nanorods due to spontaneous polarization charge (IEEE- Nano) doi: 10.1109/NANO.2015.7388917	27-30 July, 2015	Rome, Italy	Scientific Community		World
12	Conference and publication - EuroSimE	Rolanas Dauksevicius	Finite Element Modeling of ZnO Nanowire with Different Configurations of Electrodes Connected to External Capacitive Circuit for Pressure Sensing Applications (IEEE) doi: 10.1109/EuroSimE.2015.7103134	19-22 Apr. 2015	Budapest, Hungary	Scientific Community		EU
13	PhD thesis	Róbert Erdélyi	Synthesis and mechanical characterization of wet chemically grown ZnO nanowires for nanoelectromechanical sensors	Dec 2014	Veszprém, Hungary	Scientific Community		Hungary

14	Conference: - Nano S&T 2017 (accepted, oral)	Emmanuelle Pauliac-Vaujour	Challenges of Nanosystem Architectures: Realistic Paths to Multi-Scale, Multi-Modality Integration	Oct. 2017	Fukuoka, Japan	Scientific Community		World
15	Conference - Eurosensors XXXI	Elise Saoutieff	Axially stressed piezoelectric nanowires for high resolution tactile imaging	Sept. 2017	Paris, France	Scientific Community		EU
16	Conference: - European Polymer Congress (accepted, oral)	Alain Graillet	Design of UV-Crosslinked Polymeric Thin Layers for Encapsulation of Piezoelectric ZnO Nanowires for Pressure-Based Fingerprint Sensors	July 2017	Lyon, France	Scientific Community		EU
17	Conference - Annual Conference of the DPG and DPG Spring Meeting	Alexander Shkurmanov	Al-doped ZnO nanowires grown by PLD	March 2017	Dresden, Germany	Scientific Community		EU
18	Conference - Eurosensors XXX (oral)	János Volk	Integrated Piezoelectric Nanowire Arrays for High Resolution Tactile Mapping	Sept. 2016	Budapest, Hungary	Scientific Community		EU
19	Workshop - PiezoMat Workshop 2016	Antoine Viana	Introduction of the PiezoMAT EU FP7 project	Sept. 2016	Budapest, Hungary	Scientific Community		EU
20	Workshop - PiezoMat Workshop 2016	Marjolaine Allain	Heterogeneous integration of nano-objects onto microelectronics chips in CEA clean rooms	Sept. 2016	Budapest, Hungary	Scientific Community		EU
21	Workshop - PiezoMat Workshop 2016	Stéphane Revelin	High resolution fingerprint sensing – next generation in biometric identification	Sept. 2016	Budapest, Hungary	Scientific Community		EU
22	Workshop - PiezoMat Workshop 2016	Chris Sturm	On chip integration of piezoelectric nanowires	Sept. 2016	Budapest, Hungary	Scientific Community		EU
23	Workshop - PiezoMat Workshop 2016	Alain Graillet	On demand Functional polymers and materials for optoelectronic devices and sensors	Sept. 2016	Budapest, Hungary	Scientific Community		EU
24	Workshop - PiezoMat Workshop 2016	Vadim Lebedev	Piezo-electro-mechanical characterization of nano-wire sensor structures	Sept. 2016	Budapest, Hungary	Scientific Community		EU
25	Workshop - PiezoMat Workshop 2016	Nikolai Petkov	Nanowire devices for beyond CMOS technologies: lithography contacting challenges	Sept. 2016	Budapest, Hungary	Scientific Community		EU
26	Conference - Scientific Module 2016-T6 (poster)	Alexander Shkurmanov	Tilted nanowires as building block for hyperbolic metamaterials	Sep 2016	Leipzig, Germany	Scientific Community		EU
27	Conference: - Intl. Conference on Nanogenerators and Piezotronics 2016 (oral)	Elise Saoutieff	Interconnected array of piezoelectric nanowires integrated onto a microelectronics chip: the PIEZOMAT project	June 2016	Rome, Italy	Scientific Community		World
28	Conference: - Intl. Conference on Nanogenerators and Piezotronics 2016 (oral)	János Volk	Bottom contacted piezoelectric nanowire arrays for high resolution tactile mapping	June 2016	Rome, Italy	Scientific Community		World

29	Conference: - <i>Intl. Conference on Nanogenerators and Piezotronics 2016</i> (oral)	Edgar A. A. Leon Perez	On-chip integration of individually contacted piezoelectric nanowires for fingerprint sensing applications	June 2016	Rome, Italy	Scientific Community		World
30	Conference - <i>Intl. Conference on Nanogenerators and Piezotronics 2016</i> (poster)	Alexander Shkurmanov	Controlling of the geometrical shape of ZnO nanowires by pulsed laser deposition	June 2016	Rome, Italy	Scientific Community		EU
31	Conference - 2016 E-MRS Spring Meeting	Alexander Shkurmanov	Growth of ultrathin ZnO nanowires at CMOS compatible temperature by pulsed laser deposition	May 2016	Lille, France	Scientific Community		EU
32	Conference - Annual Conference of the DPG and DPG Spring Meeting	Alexander Shkurmanov	Growth of tilted ZnO nanowires by PLD on pre-structured sapphire substrates	March 2016	Regensburg, Germany	Scientific Community		EU
33	Conference - Annual Conference of the DPG and DPG Spring Meeting	Alexander Shkurmanov	CMOS-compatible PLD-growth of ultrathin ZnO nanowires	March 2016	Regensburg, Germany	Scientific Community		EU
34	Minisymposium - Quantum Coherent Structures (poster)	Alexander Shkurmanov	Growth of ultrathin ZnO nanowires	Sept-Oct 2015	Leipzig, Germany	Scientific Community		France, EU
35	Conference - Mechanical issues for advanced electron devices (poster)	Edgar A. A. Leon Perez	Bending piezoelectric nanowires: application to force-displacement sensors based on individually contacted vertical ZnO piezoelectric nanowires	July 2015	Grenoble, France	Scientific Community		France, EU
36	Conference - SETCOR NANOTECH 2015 (poster)	Edgar A. A. Leon Perez	Some design and integration considerations for piezoelectric sensors based on individually contacted vertical ZnO nanowires	June 2015	Paris, France	Scientific Community		
37	Workshop: - PiezoNEMS workshop	Elise Saoutieff	Individually contacted piezoelectric nanowires integrated onto a microelectronics chip	December 2016	Grenoble, France	Scientific Community		France, EU
38	Conference - IEEE International Conference on Nanotechnology	Edgar A. A. Leon Perez	Pixel analysis of a force-sensing device based on individually contacted vertical piezoelectric nanowires	July 2015	Rome, Italy	Scientific Community		World
39	Conference - Annual Conference of the DPG and DPG Spring Meeting (oral)	Alexander Shkurmanov	Low temperature PLD-growth of ZnO nanowires on Zn _x Al _{1-x} O films	March 2015	Berlin, Germany	Scientific Community		EU
40	Conference - TCO2014 (oral)	Alexander Shkurmanov	Low temperature PLD-growth of ZnO nanowires	Sept. 2014	Leipzig, Germany	Scientific Community		Germany, EU
41	Conference	Edgar A. A. Leon Perez	Unit-cell design of a force sensing device based on vertical piezoelectric nanowires	June 2014	Atlanta, USA	Scientific Community		World

	<i>- Intl. Conference on Nanogenerators and Piezotronics 2014 (oral)</i>							
42	<i>Conference - 10th Intern.Nanotechnology Conference on Communication and Cooperation (poster)</i>	<i>János Volk</i>	<i>Integration of vertically aligned ZnO nanorods into novel optoelectronic and sensor devices</i>	<i>May 2014</i>	<i>Gaithersburg, USA</i>	<i>Scientific Community, Policy Makers</i>		<i>World</i>
43	<i>Seminar: - PolyRay (poster)</i>	<i>Specific Polymers</i>	<i>R&D – Production – 1 g/1 kg Monomers & Polymers Fonctionnels</i>	<i>March 2014</i>	<i>Montpellier, France</i>	<i>Scientific Community</i>		<i>France, EU</i>
44	<i>Press Release</i>	<i>ULEI</i>	<i>Neuer Fingerabdrucksensor soll Sicherheit in Biometrie verbessern - Projekt PiezoMAT gestartet</i>	<i>2014</i>	<i>Leipzig, Germany</i>	<i>Public</i>		<i>Germany, EU</i>
45	<i>Press Release</i>	<i>CEA Leti</i>	<i>Leti and Partners in PIEZOMAT Project Target New Fingerprint Technology for Highly Reliable Security and ID Applications</i>	<i>2014</i>	<i>Grenoble, France</i>	<i>Public</i>		<i>World</i>

Section B (Confidential¹⁵ or public: confidential information to be marked clearly)

Part B1

TEMPLATE B1: LIST OF APPLICATIONS FOR PATENTS, TRADEMARKS, REGISTERED DESIGNS, ETC.					
Type of IP Rights ¹⁶ :	Confidential Click on YES/NO	Foreseen embargo date dd/mm/yyyy	Application reference(s) (e.g. EP123456)	Subject or title of application	Applicant (s) (as on the application)

¹⁵ Note to be confused with the "EU CONFIDENTIAL" classification for some security research projects.

¹⁶ A drop down list allows choosing the type of IP rights: Patents, Trademarks, Registered designs, Utility models, Others.

Part B2

Please complete the table hereafter:

Type of Exploitable Foreground ¹⁷	Description of exploitable foreground	Confidential Click on YES/NO	Foreseen embargo date dd/mm/yy	Exploitable product(s) or measure(s)	Sector(s) of application ¹⁸	Timetable, commercial or any other use	Patents or other IPR exploitation (licences)	Owner & Other Beneficiary(s) involved
	<i>Ex: New superconductive Nb-Ti alloy</i>			<i>MRI equipment</i>	<i>1. Medical 2. Industrial inspection</i>	<i>2008 2010</i>	<i>A materials patent is planned for 2006</i>	<i>Beneficiary X (owner) Beneficiary Y, Beneficiary Z, Poss. licensing to equipment manuf. ABC</i>

¹⁹ A drop down list allows choosing the type of foreground: General advancement of knowledge, Commercial exploitation of R&D results, Exploitation of R&D results via standards, exploitation of results through EU policies, exploitation of results through (social) innovation.

¹⁸ A drop down list allows choosing the type sector (NACE nomenclature) : http://ec.europa.eu/competition/mergers/cases/index/nace_all.html

6. Report on societal implications

Replies to the following questions will assist the Commission to obtain statistics and indicators on societal and socio-economic issues addressed by projects. The questions are arranged in a number of key themes. As well as producing certain statistics, the replies will also help identify those projects that have shown a real engagement with wider societal issues, and thereby identify interesting approaches to these issues and best practices. The replies for individual projects will not be made public.

A General Information <i>(completed automatically when Grant Agreement number is entered.)</i>	
Grant Agreement Number:	611019
Title of Project:	PiezoMat
Name and Title of Coordinator:	Dr Antoine Viana
B Ethics	
1. Did your project undergo an Ethics Review (and/or Screening)? <ul style="list-style-type: none"> If Yes: have you described the progress of compliance with the relevant Ethics Review/Screening Requirements in the frame of the periodic/final project reports? <p>Special Reminder: the progress of compliance with the Ethics Review/Screening Requirements should be described in the Period/Final Project Reports under the Section 3.2.2 'Work Progress and Achievements'</p>	0Yes 0No
2. Please indicate whether your project involved any of the following issues (tick box) :	NO
RESEARCH ON HUMANS	
• Did the project involve children?	NO
• Did the project involve patients?	NO
• Did the project involve persons not able to give consent?	NO
• Did the project involve adult healthy volunteers?	NO
• Did the project involve Human genetic material?	NO
• Did the project involve Human biological samples?	NO
• Did the project involve Human data collection?	NO
RESEARCH ON HUMAN EMBRYO/FOETUS	
• Did the project involve Human Embryos?	NO
• Did the project involve Human Foetal Tissue / Cells?	NO
• Did the project involve Human Embryonic Stem Cells (hESCs)?	NO
• Did the project on human Embryonic Stem Cells involve cells in culture?	NO
• Did the project on human Embryonic Stem Cells involve the derivation of cells from Embryos?	NO
PRIVACY	
• Did the project involve processing of genetic information or personal data (eg. health, sexual lifestyle, ethnicity, political opinion, religious or philosophical conviction)?	NO
• Did the project involve tracking the location or observation of people?	NO
RESEARCH ON ANIMALS	
• Did the project involve research on animals?	NO

• Were those animals transgenic small laboratory animals?	NO
• Were those animals transgenic farm animals?	NO
• Were those animals cloned farm animals?	NO
• Were those animals non-human primates?	NO
RESEARCH INVOLVING DEVELOPING COUNTRIES	
• Did the project involve the use of local resources (genetic, animal, plant etc)?	NO
• Was the project of benefit to local community (capacity building, access to healthcare, education etc)?	NO
DUAL USE	
• Research having direct military use	NO
• Research having the potential for terrorist abuse	NO

C Workforce Statistics

3. Workforce statistics for the project: Please indicate in the table below the number of people who worked on the project (on a headcount basis).

Type of Position	Number of Women	Number of Men
Scientific Coordinator		1
Work package leaders	1	6
Experienced researchers (i.e. PhD holders)		10
PhD Students	1	3
Other	5	3

4. How many additional researchers (in companies and universities) were recruited specifically for this project?	
Of which, indicate the number of men:	0

D Gender Aspects			
5. Did you carry out specific Gender Equality Actions under the project?	<input type="radio"/> <input checked="" type="radio"/>		Yes No
6. Which of the following actions did you carry out and how effective were they?			
Not effective	at	all	Very effective
<input type="checkbox"/> Design and implement an equal opportunity policy		○ ○ ○ ○ ○	
<input type="checkbox"/> Set targets to achieve a gender balance in the workforce		○ ○ ○ ○ ○	
<input type="checkbox"/> Organise conferences and workshops on gender		○ ○ ○ ○ ○	
<input type="checkbox"/> Actions to improve work-life balance		○ ○ ○ ○ ○	
<input type="radio"/> Other:			
7. Was there a gender dimension associated with the research content – i.e. wherever people were the focus of the research as, for example, consumers, users, patients or in trials, was the issue of gender considered and addressed?			
<input type="radio"/> Yes- please specify 			
<input checked="" type="radio"/> No			
E Synergies with Science Education			
8. Did your project involve working with students and/or school pupils (e.g. open days, participation in science festivals and events, prizes/competitions or joint projects)?			
<input type="radio"/> Yes- please specify 			
<input checked="" type="radio"/> No			
9. Did the project generate any science education material (e.g. kits, websites, explanatory booklets, DVDs)?			
<input type="radio"/> Yes- please specify 			
<input checked="" type="radio"/> No			
F Interdisciplinarity			
10. Which disciplines (see list below) are involved in your project?			
<input checked="" type="radio"/> Main discipline ¹⁹ : 2.3			
<input checked="" type="radio"/> Associated discipline ¹⁹ : 1.1			
		<input type="radio"/>	Associated discipline ¹⁹ :
G Engaging with Civil society and policy makers			
11a Did your project engage with societal actors beyond the research community? (if 'No', go to Question 14)			<input type="radio"/> <input checked="" type="radio"/>
			Yes No
11b If yes, did you engage with citizens (citizens' panels / juries) or organised civil society (NGOs, patients' groups etc.)?			
<input checked="" type="radio"/> No			
<input type="radio"/> Yes- in determining what research should be performed			
<input type="radio"/> Yes - in implementing the research			
<input type="radio"/> Yes, in communicating /disseminating / using the results of the project			

11c In doing so, did your project involve actors whose role is mainly to organise the dialogue with citizens and organised civil society (e.g. professional mediator; communication company, science museums)?		<input type="radio"/> Yes <input checked="" type="radio"/> No
12. Did you engage with government / public bodies or policy makers (including international organisations)		
<input checked="" type="radio"/> No <input type="radio"/> Yes- in framing the research agenda <input type="radio"/> Yes - in implementing the research agenda <input type="radio"/> Yes, in communicating /disseminating / using the results of the project		
13a Will the project generate outputs (expertise or scientific advice) which could be used by policy makers?		
<input type="radio"/> Yes – as a primary objective (please indicate areas below- multiple answers possible) <input type="radio"/> Yes – as a secondary objective (please indicate areas below - multiple answer possible) <input checked="" type="radio"/> No		
13b If Yes, in which fields?		
Agriculture Audiovisual and Media Budget Competition Consumers Culture Customs Development Economic and Monetary Affairs Education, Training, Youth Employment and Social Affairs		Energy Enlargement Enterprise Environment External Relations External Trade Fisheries and Maritime Affairs Food Safety Foreign and Security Policy Fraud Humanitarian aid
		Human rights Information Society Institutional affairs Internal Market Justice, freedom and security Public Health Regional Policy Research and Innovation Space Taxation Transport

¹⁹ Insert number from list below (Frascati Manual).

13c If Yes, at which level? <ul style="list-style-type: none"> <input type="radio"/> Local / regional levels <input type="radio"/> National level <input type="radio"/> European level <input type="radio"/> International level 		
H Use and dissemination		
14. How many Articles were published/accepted for publication in peer-reviewed journals?		
To how many of these is open access²⁰ provided?		
How many of these are published in open access journals?		
How many of these are published in open repositories?		
To how many of these is open access not provided?		
Please check all applicable reasons for not providing open access:		
<input type="checkbox"/> publisher's licensing agreement would not permit publishing in a repository <input type="checkbox"/> no suitable repository available <input type="checkbox"/> no suitable open access journal available <input type="checkbox"/> no funds available to publish in an open access journal <input type="checkbox"/> lack of time and resources <input type="checkbox"/> lack of information on open access <input type="checkbox"/> other ²¹ :		
15. How many new patent applications ('priority filings') have been made? <i>("Technologically unique": multiple applications for the same invention in different jurisdictions should be counted as just one application of grant).</i>		0
16. Indicate how many of the following Intellectual Property Rights were applied for (give number in each box).	Trademark	
	Registered design	
	Other	
17. How many spin-off companies were created / are planned as a direct result of the project?		0
<i>Indicate the approximate number of additional jobs in these companies:</i>		
18. Please indicate whether your project has a potential impact on employment, in comparison with the situation before your project:		
<input type="checkbox"/> Increase in employment, or <input type="checkbox"/> Safeguard employment, or <input type="checkbox"/> Decrease in employment, <input checked="" type="checkbox"/> Difficult to estimate / not possible to quantify	<input type="checkbox"/> In small & medium-sized enterprises <input type="checkbox"/> In large companies <input type="checkbox"/> None of the above / not relevant to the project	

²⁰ Open Access is defined as free of charge access for anyone via Internet.

²¹ For instance: classification for security project.

<p>19. For your project partnership please estimate the employment effect resulting directly from your participation in Full Time Equivalent (FTE = one person working fulltime for a year) jobs:</p> <p>Difficult to estimate / not possible to quantify</p>	<p><i>Indicate figure:</i></p> <p>■</p>												
<p>I Media and Communication to the general public</p>													
<p>20. As part of the project, were any of the beneficiaries professionals in communication or media relations?</p> <p><input type="radio"/> Yes <input checked="" type="radio"/> No</p>													
<p>21. As part of the project, have any beneficiaries received professional media / communication training / advice to improve communication with the general public?</p> <p><input type="radio"/> Yes <input checked="" type="radio"/> No</p>													
<p>22 Which of the following have been used to communicate information about your project to the general public, or have resulted from your project?</p> <table border="0"> <tr> <td><input checked="" type="checkbox"/> Press Release</td> <td><input type="checkbox"/> Coverage in specialist press</td> </tr> <tr> <td><input type="checkbox"/> Media briefing</td> <td><input type="checkbox"/> Coverage in general (non-specialist) press</td> </tr> <tr> <td><input type="checkbox"/> TV coverage / report</td> <td><input checked="" type="checkbox"/> Coverage in national press</td> </tr> <tr> <td><input type="checkbox"/> Radio coverage / report</td> <td><input type="checkbox"/> Coverage in international press</td> </tr> <tr> <td><input type="checkbox"/> Brochures /posters / flyers</td> <td><input checked="" type="checkbox"/> Website for the general public / internet</td> </tr> <tr> <td><input type="checkbox"/> DVD /Film /Multimedia</td> <td><input checked="" type="checkbox"/> Event targeting general public (festival, conference, exhibition, science café)</td> </tr> </table>		<input checked="" type="checkbox"/> Press Release	<input type="checkbox"/> Coverage in specialist press	<input type="checkbox"/> Media briefing	<input type="checkbox"/> Coverage in general (non-specialist) press	<input type="checkbox"/> TV coverage / report	<input checked="" type="checkbox"/> Coverage in national press	<input type="checkbox"/> Radio coverage / report	<input type="checkbox"/> Coverage in international press	<input type="checkbox"/> Brochures /posters / flyers	<input checked="" type="checkbox"/> Website for the general public / internet	<input type="checkbox"/> DVD /Film /Multimedia	<input checked="" type="checkbox"/> Event targeting general public (festival, conference, exhibition, science café)
<input checked="" type="checkbox"/> Press Release	<input type="checkbox"/> Coverage in specialist press												
<input type="checkbox"/> Media briefing	<input type="checkbox"/> Coverage in general (non-specialist) press												
<input type="checkbox"/> TV coverage / report	<input checked="" type="checkbox"/> Coverage in national press												
<input type="checkbox"/> Radio coverage / report	<input type="checkbox"/> Coverage in international press												
<input type="checkbox"/> Brochures /posters / flyers	<input checked="" type="checkbox"/> Website for the general public / internet												
<input type="checkbox"/> DVD /Film /Multimedia	<input checked="" type="checkbox"/> Event targeting general public (festival, conference, exhibition, science café)												
<p>23 In which languages are the information products for the general public produced?</p> <table border="0"> <tr> <td><input checked="" type="checkbox"/> Language of the coordinator</td> <td><input checked="" type="checkbox"/> English</td> </tr> <tr> <td><input type="checkbox"/> Other language(s)</td> <td></td> </tr> </table>		<input checked="" type="checkbox"/> Language of the coordinator	<input checked="" type="checkbox"/> English	<input type="checkbox"/> Other language(s)									
<input checked="" type="checkbox"/> Language of the coordinator	<input checked="" type="checkbox"/> English												
<input type="checkbox"/> Other language(s)													